









Cite this: *Dalton Trans.*, 2019, **48**,  
3249

## A biocompatible redox MRI probe based on a Mn(II)/Mn(III) porphyrin†

Sara M. A. Pinto, \*<sup>a,b</sup> Mário J. F. Calvete, <sup>a,b</sup> Mariana E. Ghica,<sup>a</sup> Sérgio Soler,<sup>c</sup> Iluminada Gallardo, <sup>c</sup> Agnès Pallier,<sup>d</sup> Mariana B. Laranjo,<sup>b,e</sup> Ana M. S. Cardoso,<sup>f</sup> M. Margarida C. A. Castro, <sup>b,e</sup> Christopher M. A. Brett, <sup>a</sup> Mariette M. Pereira, \*<sup>a,b</sup> Éva Tóth \*<sup>d</sup> and Carlos F. G. C. Geraldès \*<sup>b,e</sup>

For the development of redox responsive MRI probes based on the Mn<sup>III</sup>/Mn<sup>II</sup> couple, stable complexation of both reduced and oxidized forms of the metal ion and appropriate tuning of the redox potential in the biologically relevant range are key elements. The water soluble fluorinated Mn-porphyrin derivative Mn-**3** satisfies both requirements. In aqueous solutions, it can reversibly switch between Mn<sup>III</sup>/Mn<sup>II</sup> oxidation states. In the presence of ascorbic acid or β-mercaptoethanol, the Mn<sup>III</sup> form undergoes reduction, which is slowly but fully reversed in the presence of air oxygen. A UV-Vis kinetic study of Mn<sup>III</sup>/Mn<sup>II</sup> reduction under oxygen-free conditions yielded second-order rate constants,  $k_2$ , of 46.1 M<sup>-1</sup> s<sup>-1</sup> and 13.8 M<sup>-1</sup> s<sup>-1</sup> for the reaction with ascorbic acid and β-mercaptoethanol, respectively. This could correspond, in the absence of oxygen, to a half-life of a few minutes in blood plasma and a few seconds in circulating immune cells where ascorbic acid reaches 20–40 μM and a few mM concentrations, respectively. In contrast to expectations based on the redox potential, reduction with glutathione or cysteine does not occur. It is prevented by the coordination of the glutathione carboxylate group(s) to Mn<sup>III</sup> in the axial position, as was evidenced by NMR data. Therefore, Mn<sup>III</sup>-**3** acts as an ascorbate specific turn-on MRI probe, which in turn can be re-oxidized by oxygen. The relaxivity increase from the oxidized to the reduced form is considerably improved at medium frequencies (up to 80 MHz) with respect to the previously studied Mn-TPPS<sub>4</sub> analogues; at 20 MHz, it amounts to 150%. No *in vitro* cytotoxicity is detectable for Mn-**3** in the typical MRI concentration range. Finally, <sup>19</sup>F NMR resonances of Mn<sup>III</sup>-**3** are relatively sharp which could open further opportunities to exploit such complexes as paramagnetic <sup>19</sup>F NMR probes.

Received 3rd December 2018,  
Accepted 29th January 2019

DOI: 10.1039/c8dt04775h

rsc.li/dalton

<sup>a</sup>Department of Chemistry, Faculty of Science and Technology, University of Coimbra, Rua Larga, 3004-535, Coimbra, Portugal. E-mail: smpinto@qui.uc.pt<sup>b</sup>Coimbra Chemistry Centre, CQC, University of Coimbra, Rua Larga, 3004-535, Coimbra, Portugal. E-mail: geraldès@ci.uc.pt<sup>c</sup>Departament de Química, Universitat Autònoma de Barcelona, 08193 BellaterraBarcelona, Spain<sup>d</sup>Centre de Biophysique Moléculaire, CNRS, UPR 4301, Université d'Orléans, Orléans, France. E-mail: Eva.JAKABTOTH@cnrs.fr<sup>e</sup>Department of Life Sciences, Faculty of Science and Technology, University of Coimbra, Calçada Martim de Freitas, 3000-393, Coimbra, Portugal<sup>f</sup>Center of Neurosciences and Cell Biology, CNC, University of Coimbra, Rua Larga, Faculty of Medicine, 3004-504, Coimbra, Portugal

† Electronic supplementary information (ESI) available: Fig. S1–S12: <sup>1</sup>H, <sup>19</sup>F NMR and ESI-FIA-TOF mass spectra of porphyrin **2**; ESI-FIA-TOF mass spectra of Mn<sup>III</sup>-**3**; EPR spectra of MnCl<sub>2</sub> and Mn<sup>III</sup>-**3** in PBS (pH 7.4) at 25 °C; <sup>1</sup>H and <sup>19</sup>F NMR spectra of Mn<sup>III</sup>-**3** and Mn<sup>II</sup>-**3** in CDCl<sub>3</sub>; cyclic voltammograms of Zn<sup>II</sup>-**3** and Mn<sup>III</sup>-**3**; UV-Vis spectra of the re-oxidation of Mn<sup>II</sup>-**3** with hydrogen peroxide; UV-Vis spectrum of 0.041 mM Mn<sup>III</sup>-**3** and of Mn<sup>II</sup>-**3** 24 h after addition of 25.3 equivalents of ascorbic acid; kinetic results for the reduction of Mn<sup>III</sup>-**3** to Mn<sup>II</sup>-**3** with ascorbic acid and with mercaptoethanol in PBS (25 °C, pH = 7.4); <sup>13</sup>C NMR of glutathione without and with 0.1 equiv. of Mn<sup>III</sup>-**3** in D<sub>2</sub>O; Table S1: reduction potentials of Zn<sup>II</sup>-**3** and Mn<sup>III</sup>-**3** and comparison with the literature values for some perfluorinated tetraphenylporphyrins. Equations used to analyze the <sup>1</sup>H NMRD profiles. See DOI: 10.1039/c8dt04775h

## Introduction

In any living body, both extracellular and intracellular redox environments are tightly regulated<sup>1–3</sup> and their dysregulation may be associated with a wide range of pathophysiological conditions, including chronic inflammation,<sup>4</sup> neoplastic growth<sup>5</sup> and ischemia,<sup>6</sup> since several triggered biochemical cascade events can damage cellular or tissue components, promoting disease progression.<sup>7–9</sup> The redox environment in a biological fluid, organelle, cell, or tissue is maintained by a number of redox couples present which are linked to each other. Among these, glutathione (GSH) is the major thiol-disulfide redox buffer of the cell with an average concentration of 1–11 mM in the cytosol, much higher than those of most other redox active compounds.<sup>10</sup> Therefore, the redox state of the glutathione disulfide–glutathione couple (GSSG/2GSH) can serve as an indicator of the intracellular redox environment. Changes of the half-cell reduction potential ( $E_{hc}$ ) of the GSSG/2GSH couple appear to correlate with the biological status of the cell: proliferation  $E_{hc} \sim -240$  mV; differentiation  $E_{hc} \sim -200$  mV;

or apoptosis  $E_{hc} \sim -170$  mV.<sup>10</sup> The extracellular space is typically more oxidized than the cytosol. In cell extracts, the total concentrations of reduced (GSH) and oxidized (GSSG) glutathione present can be assessed by HPLC or fluorescence assays.<sup>11,12</sup>

The development of imaging techniques capable of following an *in vivo* tissue redox environment/activity is of utmost interest in clinical research and medical practice, particularly in diagnosis, prognosis or monitoring therapeutic response.<sup>13,14</sup> The fundamental goal of developing molecular probes capable of imaging redox activity has seen some clinical success. In particular, positron emission tomography (PET) probes capable of targeting hypoxic tissue, such as the radiotracers  $^{64}\text{Cu}^{\text{II}}$ -diacetyl-bis(*N*4-methylthiosemi-carbazone) ( $^{64}\text{Cu}^{\text{II}}$ -ATSM) and  $^{18}\text{F}$ -fluoro-misonidazole ( $^{18}\text{F}$ -MISO), showed a capacity to predict the treatment outcome in patients undergoing radiotherapy.<sup>15–17</sup> The same hypoxia targeting mechanism of probe uptake (irreversible reaction and retention in oxygen-deprived tissue) has been extended to MRI contrast agents and fluorescent probes for optical imaging.<sup>18,19</sup> Redox-sensitive nitroxide derivative probes were also used in electron paramagnetic resonance (EPR) imaging and spectroscopy to detect a reductive environment (thiols and other reducing species).<sup>20,21</sup>

Magnetic resonance imaging (MRI) is an attractive modality to monitor redox dynamics thanks to its exceptional spatial resolution (<100  $\mu\text{m}$  using modern high-field equipment), lack of invasiveness and use of ionizing radiation, and its ability to simultaneously report physiological and anatomical information. Not surprisingly, the interest in the development of redox sensitive MRI probes has grown over the last few years.<sup>14,22–26</sup> These can be based on redox active ligands, undergoing a change in the ligand structure or the molecular rotation upon reduction/oxidation, while the oxidation state of the paramagnetic metal remains the same (*e.g.* a merocyanine unit linked to GdDO3A which isomerizes to the spirooxazine derivative by the redox stimulus of NADH).<sup>27</sup> Alternatively, complexes of redox active paramagnetic metals, such as europium and manganese, can also be explored, in which the different oxidation states have different magnetic properties.<sup>11,22</sup> Altogether, both types of probes must fulfill several requirements: (i) biocompatibility, (ii) a redox half-cell potential which is compatible with the redox potential of biological reducing agents; (iii) strong signal change, and if possible a signal increase upon activation (“turn-on” probe); and (iv) rapid redox kinetics as compared to the imaging time scale. Importantly, the redox active metal ion needs to be complexed by a ligand that is capable of efficiently chelating both oxidation states so that reduction or oxidation does not result in the decomposition of the complex.

Among redox active metal ions, manganese is particularly attractive for the development of redox responsive MRI probes, whose efficiency is measured from their proton relaxivity  $r_i$  ( $i = 1, 2$ ) (paramagnetic enhancement of the water proton relaxation rates,  $R_i = T_i^{-1}$ , where  $T_1$  and  $T_2$  are, respectively, the longitudinal and transverse relaxation times, referred to a

1 mM concentration of the paramagnetic ion). Manganese is a biogenic element and in its +2 oxidation state,  $\text{Mn}^{2+}$ , it is a very efficient paramagnetic relaxation agent.  $\text{Mn}^{2+}$  ( $d^5$  configuration, high spin  $S = 5/2$ ), with long (in the 0.1–1 ns range) longitudinal electronic relaxation times and labile water exchange, is an attractive alternative to  $\text{Gd}^{3+}$  in MRI probes.<sup>28,29</sup> Indeed, in the last few years, there has been intensive research to identify suitable ligand structures for  $\text{Mn}^{2+}$  chelation.<sup>30,31</sup>  $\text{Mn}^{3+}$  ( $d^4$  configuration) is also paramagnetic, usually giving rise to high spin  $S = 2$  compounds. While water exchange is also fast,<sup>14</sup> the longitudinal electronic relaxation times are shorter ( $\leq 10$  ps), making them less efficient relaxation agents.<sup>32</sup> The nuclear relaxation mechanism of  $\text{Mn}^{3+}$  is different from that of  $\text{Mn}^{2+}$  and therefore their relaxation efficiency shows a very distinct dependence on the external magnetic field  $B_0$ . While for the  $S = 5/2$   $\text{Mn}^{2+}$  complexes, the classical Solomon–Bloembergen–Morgan (SBM) formalism describes well nuclear relaxation, leading to a decrease of  $r_1$  at a high field, for the  $S = 2$   $\text{Mn}^{3+}$  complexes the analysis of the water proton relaxation rates is much less straightforward. Water soluble and air stable  $\text{Mn}^{3+}$ -porphyrins have been investigated as tumor targeted MRI agents.<sup>33</sup> For these compounds, the electron relaxation times are relatively long due to their higher symmetry.<sup>32</sup> For instance, the  $\text{Mn}^{\text{III}}$ -TPPS<sub>4</sub> (*meso*-tetra(4-sulfonatophenyl)porphine chloride)chelate<sup>34</sup> displays an anomalous  $r_1$  relaxivity, with a peak above approximately 2 MHz. It was shown that the NMR relaxation mechanism has several unique aspects, including the unusual role of large rhombic zero-field splitting (ZFS) interactions, which are of the order of the nuclear Zeeman energy. The effect of these interactions on the electron spin dynamics leads to these relaxivity anomalies at a high field.<sup>35,36</sup> As a consequence of the different relaxation mechanisms, the proton relaxivity, and thus the MRI efficiency can be either higher or lower for the reduced  $\text{Mn}^{2+}$  relative to the oxidized  $\text{Mn}^{3+}$  form, depending on the external magnetic field and on the chelating ligand.

Porphyrins, which are macrocyclic ligands par excellence and widely used in a multitude of applications, such as catalysis,<sup>37–39</sup> materials science<sup>40–46</sup> and biomedicine, including MRI,<sup>30,47–51</sup> offer the possibility to obtain very stable chelates to host many metal ions, including paramagnetic ones. Such metalloporphyrins having a much reduced risk of transmetallation may avoid potential *in vivo* metal release during the MRI examination which would cause toxicity, such as gadolinium induced fibrosis disorders,<sup>52</sup> or manganese induced neurotoxicity.<sup>50,51,53</sup> Many studies have been reported on  $\text{Mn}^{\text{III}}$ -porphyrin dimers, and supramolecular and macromolecular conjugates as MRI contrast agents,<sup>33,54–61</sup> including enzyme<sup>58,59</sup> and  $\text{Zn}^{2+}$ -responsive<sup>60,61</sup> agents. So far, the only studies on Mn-porphyrins as redox MRI probes have been reported by Aime and collaborators,<sup>62</sup> who explored a  $\text{Mn}^{\text{II}}/\text{Mn}^{\text{III}}$ -based water-soluble porphyrin (TPPS<sub>4</sub>) as an oxygen sensor. However, at clinically relevant fields ( $^1\text{H}$  frequencies of 60–120 MHz), and at 25 °C, the  $r_1$  relaxivity values were revealed to be very close for the  $\text{Mn}^{\text{II}}$  and  $\text{Mn}^{\text{III}}$  analogues. On the other hand, the formation of macromolecular conjugates,

through the encapsulation of the  $\text{Mn}^{\text{II}}$ -TPPS<sub>4</sub> and  $\text{Mn}^{\text{III}}$ -TPPS<sub>4</sub> complexes in commercially available, water-soluble poly- $\beta$ -cyclodextrin (CD), led to a marked difference in the relaxivities at 20 MHz between the reduced and oxidized states.

Caravan and collaborators<sup>30</sup> explored hydroxybenzylethyl-enediamine acetic acid derivatives for  $\text{Mn}^{\text{II/III}}$ -chelation to create redox active contrast agents. The stability of the complexes was recently improved by using a "Janus" ligand that readily isomerizes between binding modes that favor either the  $\text{Mn}^{3+}$  or  $\text{Mn}^{2+}$  ion.<sup>30</sup> Rapid and reversible interconversion between the two oxidation modes was achieved by peroxidase activity (oxidation) and L-cysteine (reduction), which was translated into an unprecedented 9-fold relaxivity increase between the  $\text{Mn}^{3+}$  and  $\text{Mn}^{2+}$  analogues, respectively. One concern, nevertheless, about these open-chain complexes is the lack of a sufficiently high kinetic inertness which is desirable for *in vivo* applications.

Based on previous experience in porphyrin chemistry, our objective is to develop water soluble, biocompatible Mn-porphyrin complexes with a redox potential that is adapted to biological requirements. The approach to the development of such specifically designed  $\text{Mn}^{\text{II/III}}$  complexes involves modulating the redox potential by using appropriate electron withdrawing substituents on the porphyrin structure. The fine-tuning of the redox potential would be highly important since most of the redox responsive MRI probes reported so far do not undergo redox chemistry in a biologically relevant range.<sup>22</sup> The capacity of porphyrin complexes to selectively localize in tumor cells is well known and will be a great advantage. Indeed, it can simplify the probe design as no additional targeting and cell internalizing moieties are required, although they might be later added to the chemical structure to further improve these properties.

Herein we report the synthesis and physical-chemical characterization of a new fluorinated  $\text{Mn}^{\text{II/III}}$  porphyrin derivative which was conjugated with PEG chains for better solubility

and biocompatibility. Its redox properties were studied by cyclic voltammetry. The  $\text{Mn}^{\text{III}}$  reduction kinetics was followed in the presence of ascorbic acid and  $\beta$ -mercaptoethanol (BME) by UV-Vis. The relaxivity differences between the reduced and oxidized forms were investigated using <sup>1</sup>H Nuclear Magnetic Relaxation Dispersion (NMRD). Cytotoxicity evaluation of the system on epithelial HeLa cells is also reported.

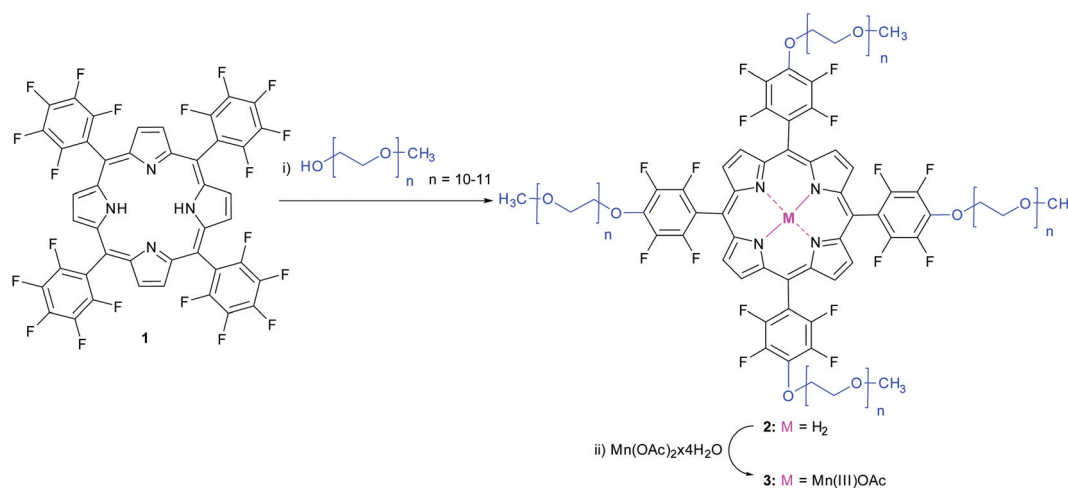
## Results and discussion

### Synthesis of the biocompatible porphyrin-based probes

The strategy adopted for the synthesis of the  $\text{Mn}^{\text{III}}$  biocompatible probe 3 is depicted in Scheme 1.

Porphyrin 1 was synthesized by the NaY method, developed by some of us,<sup>63</sup> where NaY acts as a reusable catalyst. After work-up 12% of the isolated porphyrin was obtained. In order to obtain free base porphyrin 2, nucleophilic aromatic substitution of 1 using mono-methyl protected polyethylene glycol with  $M_w = \sim 500 \text{ g mol}^{-1}$  (PEG500) was performed, in DMF as the solvent and NaH as a base, at room temperature for two hours. The product was obtained in 65% yield, after purification, and fully characterized by <sup>1</sup>H and <sup>19</sup>F NMR spectroscopy and ESI-FIA-TOF mass spectrometry (see Fig. 1 and Fig. S1–S3, ESI†). Its main characterization detailing feature was ascertained by observing the loss of the characteristic triplet (*p*-F) <sup>19</sup>F NMR signal at around  $-150 \text{ ppm}$  (Fig. 1) for porphyrin 2, when compared with the <sup>19</sup>F NMR spectrum of 1, which presents its three typical (*m*-F), (*p*-F) and (*o*-F) signals at  $-160.2$ ,  $-150.1$  and  $-135.4 \text{ ppm}$ , respectively (Fig. 1), confirming the tetrapegylation pattern obtained.

The preparation of  $\text{Mn}^{\text{III}}$ -3 proceeded by reacting 2 with excess manganese diacetate tetrahydrate in sodium acetate/acetic acid buffer solution at 80 °C for two hours. After several extraction processes of the crude product with dichloromethane/water, the organic layer was dried with anhydrous



**Scheme 1** Synthetic route for the preparation of the biocompatible porphyrin 3. Reagents and conditions: (i) DMF, NaH, room temperature, 2 h; (ii) acetic acid/sodium acetate,  $\text{Mn}(\text{II})$ acetate tetrahydrate, 80 °C, 2 h.

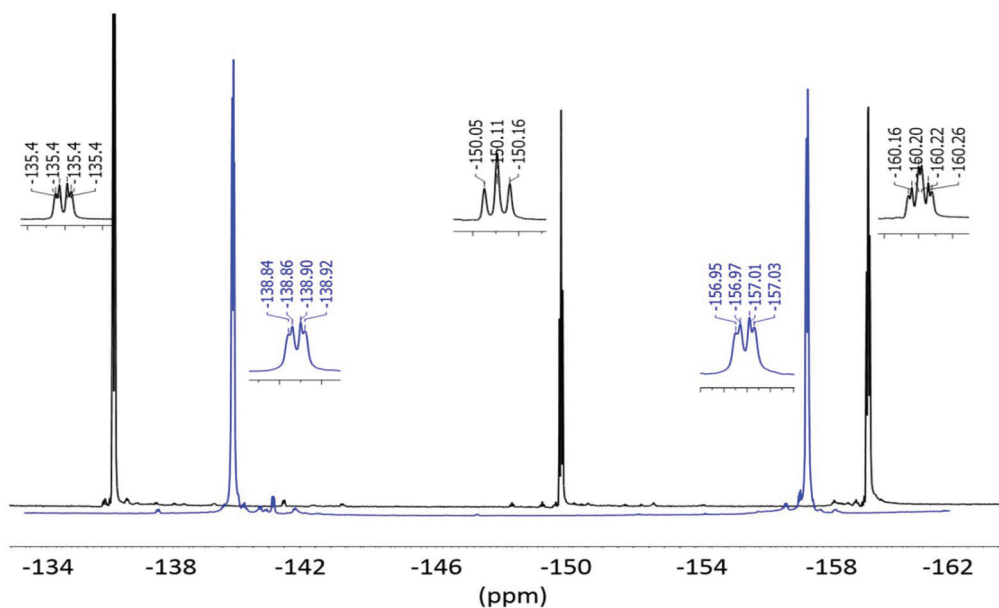


Fig. 1  $^{19}\text{F}$  NMR of porphyrin 1 (black spectrum) and porphyrin 2 (blue spectrum).

sodium sulfate and concentrated under vacuum giving **3** in 82% yield (Scheme 1). The  $\text{Mn}^{\text{III}}$ -**3** complex was characterized by ESI-FIA-TOF mass spectrometry (see Fig. S4, ESI $^\dagger$ ), presenting the characteristic poly-dispersed  $m/z$  peaks from PEGylated 1121.3612, 1319.9802, 1386.0195, and 1493.6057  $[\text{M}]^{2+}$  (poly-disperse distribution). Additionally, Electron Paramagnetic Resonance (EPR) experiments were also performed, in order to confirm the absence of the  $\text{Mn}^{\text{II}}$  salt used in the complexation reaction. The absence of the sharp sextet characteristic of the free aqueous  $\text{Mn}^{2+}$  cation even at a very high amplification, led to the conclusion that the  $\text{Mn}^{\text{III}}$ -**3** sample was free of aqueous  $\text{Mn}^{2+}$  (Fig. S5, ESI $^\dagger$ ).<sup>47</sup> The EPR spectrum of  $\text{Mn}^{\text{III}}$ -**3** was also silent at room temperature, as expected from the fast electron relaxation characteristic of the integer-spin (non-Kramers) porphyrin compound.<sup>64</sup> Characteristic EPR resonances of  $\text{Mn}^{\text{II}}$ -porphyrins have been observed at liquid nitrogen temperature (e.g. a strong sextet at  $g_\perp \sim 5.9$ – $5.2$ , a signal at  $g_\parallel \sim 2.0$ – $2.1$ , and sometimes three other weak signals at 1.23, 0.77 and 0.54).<sup>62,64</sup> If some  $\text{Mn}^{\text{II}}$ -**3** were present in the sample, a broad signal at  $g_{\text{iso}} \sim 2.0$  would be observable at room temperature,<sup>65</sup> which was not the case.

### Proton and $^{19}\text{F}$ NMR

The proton NMR spectrum of  $\text{Mn}^{\text{III}}$ -**3** in  $\text{CDCl}_3$  (Fig. S6a $^\dagger$ ) shows a broad signal at  $-22.76$  ppm corresponding to the  $\beta$ -pyrrole protons, characteristic of  $\text{Mn}^{\text{III}}$  high-spin *meso*-porphyrins. The large upfield shift and large broadening observed arise from the dominant contact mechanism, due to the small magnetic anisotropy of the coordinated  $\text{Mn}^{\text{III}}$  ion and consequent dipolar shift induced.<sup>66,67</sup> The PEG chain  $\text{CH}_2$  protons at 3.66 ppm remain unshifted and hardly broadened relative to the signal at 3.65 ppm for free PEG due to their long distance from the paramagnetic center.

The  $^{19}\text{F}$  NMR spectrum of  $\text{Mn}^{\text{III}}$ -**3** (Fig. S6b $^\dagger$ ) consists of a broad signal centered at  $-126.2$  ppm and a set of five upfield shifted (in the range of  $-149.7$  to  $-157.7$  ppm) sharper (line-widths around 190 Hz) signals of different intensities. This set of signals corresponds to the fluorine atoms at the *meta* positions of the *meso*-phenyl groups in the five possible combinations of the chain lengths of the four polydisperse PEG chains with  $n = 10$ – $11$ . The broad signal around  $-126.2$  ppm results from the overlap of the broader signals of the fluorine atoms at the *ortho* position, which are closer to the metal center.<sup>68,69</sup> Upon reduction of  $\text{Mn}^{\text{III}}$ -**3** to  $\text{Mn}^{\text{II}}$ -**3**, all the  $^{19}\text{F}$  resonances are completely broadened out, in accordance with the efficient paramagnetic relaxation of  $\text{Mn}^{\text{II}}$  (Fig. S6c $^\dagger$ ).

### Cyclic voltammetry

The electrochemical behaviour of the porphyrin TPFPP(PEG)<sub>4</sub> (**2**) and the metalloporphyrins  $\text{Mn}^{\text{III}}$ -TPFPP(PEG)<sub>4</sub> ( $\text{Mn}^{\text{III}}$ -**3**) and  $\text{Zn}^{\text{II}}$ -TPFPP(PEG)<sub>4</sub> ( $\text{Zn}^{\text{II}}$ -**3**) was investigated in deoxygenated 0.1 M HEPES buffer solution, pH 7.4, by cyclic voltammetry at a glassy carbon electrode (GCE). The cyclic voltammograms obtained for the fluorinated porphyrins are presented in Fig. 2a. No adsorption of any porphyrin was observed in consecutive cycles.

In the potential range investigated, which is limited by water reduction and oxidation potentials, the following behavior was observed. The free porphyrin exhibited two redox couples  $\text{II}_a/\text{II}_c$  and  $\text{I}_a/\text{I}_c$ , with a midpoint potential  $E_{\text{pII}}^{\text{m}} = -0.580$  V and peak separation  $\Delta E_{\text{pII}} = 0.120$  V and  $E_{\text{pI}}^{\text{m}} = -1.060$  V and peak separation  $\Delta E_{\text{pI}} = 0.120$  V, respectively. These couples were ascribed to two successive one-electron oxidation/reduction processes of the porphyrin ring, the first involving a  $\pi$ -radical anion and the second the porphyrin dianion formation, respectively, as suggested in the literature.<sup>66,70</sup> The



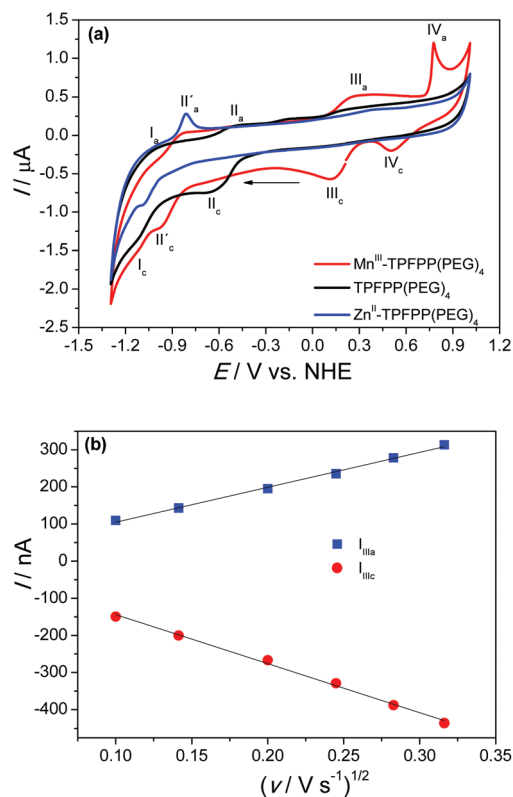


**Fig. 2** (a) Cyclic voltammograms at the GCE in 0.1 M HEPES buffer, pH 7.4, for 2.2 mM of TPFPP(PEG)<sub>4</sub> (black), Mn<sup>III</sup>-3 (red) and Zn<sup>II</sup>-3 (blue); (b) plot of the peak current versus square root of the scan rate for the peaks III<sub>a</sub>/III<sub>c</sub>, corresponding to Mn<sup>II</sup>/Mn<sup>III</sup> for the CV of 2.2 mM Mn<sup>III</sup>-3 in 0.1 M HEPES buffer, pH 7.4, at scan rates 10–100 mV s<sup>-1</sup>.

formal potential for these peaks shifted to more negative values for Mn<sup>III</sup>-3 ( $E_{\text{pIII}}^{\text{m}} = -0.900$  V), and for Zn<sup>II</sup>-3 ( $E_{\text{pIII}}^{\text{m}} = -0.945$  V) porphyrins, which is expected with the introduction of a metal ion in the porphyrin by its effect on the electronic structure of the macrocyclic ring. For Zn<sup>II</sup>-3 no additional peaks were observed in the potential range studied; those involving the oxidation of the porphyrin ring should be higher than +1.20 V (see later). In the case of Mn<sup>III</sup>-3 two more redox couples III<sub>a</sub>/III<sub>c</sub> and IV<sub>a</sub>/IV<sub>c</sub> appeared. The III<sub>a</sub>/III<sub>c</sub> pair with  $E_{\text{pIII}}^{\text{m}} = +0.193$  V and  $\Delta E_{\text{pIII}} = 0.150$  V was assigned to the Mn<sup>II</sup>/Mn<sup>III</sup> redox process, while IV<sub>a</sub>/IV<sub>c</sub> with  $E_{\text{pIV}}^{\text{m}} = +0.642$  V and  $\Delta E_{\text{pIV}} = 0.264$  V was associated with the Mn<sup>III</sup>/Mn<sup>IV</sup> reaction. These assignments were confirmed by performing cyclic voltammetry under the same conditions in the presence of Mn<sup>III</sup>-acetate (Fig. S7a†), where two redox couples also appeared. The pair IV<sub>a</sub>/IV<sub>c</sub> exhibited potential values  $E_{\text{pIV}}^{\text{m}} = +0.575$  V and  $\Delta E_{\text{pIV}} = 0.222$  V for Mn<sup>III</sup>-acetate, quite similar to those of Mn<sup>III</sup>-3 and of the cationic tetramethyl *meso*-substituted porphyrin, Mn<sup>III</sup>-PMPyP, at basic pH.<sup>71–73</sup> The reversibility of this redox process was not found to depend on experimental conditions<sup>74</sup> and will not be further discussed here. However, for the pair III<sub>a</sub>/III<sub>c</sub> a large difference was observed; the peak separation was wider,  $\Delta E_{\text{pIII}} = +0.778$  V, while the formal potential was more negative,  $E_{\text{pIII}}^{\text{m}} = -0.065$  V for Mn<sup>III</sup>-acetate. An

increase in the peak current was also observed for the same redox couple, III<sub>a</sub>/III<sub>c</sub>, a factor of 2 for the oxidation process and 3 for the reduction process in the case of the Mn<sup>III</sup>-3 porphyrin compared with Mn<sup>III</sup>-acetate. Thus, the introduction of manganese into the porphyrin has a positive impact, by greatly increasing its reversibility with regard to the Mn<sup>II</sup>/Mn<sup>III</sup> process. An improvement in the Mn<sup>II</sup>/Mn<sup>III</sup> redox reaction was also achieved when introducing manganese in a sulphonated porphyrin, Mn<sup>III</sup>-TPPS<sub>4</sub>, since this redox pair exhibited a peak separation  $\Delta E_{\text{pIII}} = 0.252$  V with a midpoint potential  $E_{\text{pIII}}^{\text{m}} = -0.238$  V (data not shown). However, the formal potential for Mn<sup>III</sup>-3 is more positive and the peaks are less separated, as well as exhibiting higher current peaks, compared with Mn<sup>III</sup>-TPPS<sub>4</sub>, which enables the former porphyrin to be elected as a better redox probe. Although the Mn<sup>II</sup>/Mn<sup>III</sup> redox reaction in Mn<sup>III</sup>-3 was a quasi-reversible slow electron transfer, this is in agreement with what was found for non-fluorinated Mn-porphyrins, e.g. Mn<sup>III</sup>-TPPS<sub>4</sub>, with  $E_{\text{pIII}}^{\text{m}}$  values of  $-0.24$  V in DMF/0.1 M TBAP<sup>75</sup> and  $-0.22$  V in water/0.3 M Na<sub>2</sub>SO<sub>4</sub>,<sup>76</sup> as well as for manganese fluorinated porphyrin, Mn-TPFPP, in acetonitrile,<sup>61</sup> with an  $E_{\text{pIII}}^{\text{m}}$  value of  $+0.05$  V (Table S1†).

The cyclic voltammetric behaviour of the Mn<sup>III</sup>-3 porphyrin was investigated over a range of scan rates from 10 to 100 mV s<sup>-1</sup>. The results showed a linear dependence of the anodic and cathodic peak currents of the redox couple Mn<sup>II</sup>/Mn<sup>III</sup> on the square root of the scan rate ( $\nu$ ) (Fig. 2b and Fig. S7b†), indicating a diffusion-controlled electron transfer process,<sup>77</sup> in agreement with what was previously observed for the complex Mn<sup>III</sup>-HBET (HBET = *N*-(2-hydroxybenzyl)-*N,N,N'*-ethylenediaminetriacetic acid)<sup>26</sup> and other manganese-based porphyrins.<sup>78</sup> The stability of the Mn<sup>III</sup>-3 porphyrin was checked by recording cyclic voltammograms of the prepared solution over a period of one month. No change in the peak current values was observed, indicating high stability of this compound in aqueous solution. In spite of the quasi-reversible process, the value of the redox potential achieved and its high stability ensure the ability of Mn<sup>III</sup>-3 to act as a redox probe, as proposed here.

The redox behaviour of the free porphyrin and the Zn<sup>II</sup>-3 and Mn<sup>III</sup>-3 derivatives was also investigated by cyclic voltammetry in DCE and 0.6 M Bu<sub>4</sub>NBF<sub>4</sub> at a glassy carbon electrode (Table S1 and Fig. S7d, e†). The free porphyrin showed two redox couples at negative potentials with  $E_{\text{p}}^{\text{m}}$  values at  $-0.452$  V and  $-1.00$  V, corresponding to the porphyrin ring anion and dianion formation. Zn<sup>II</sup>-3 showed two reversible monoelectronic reduction peaks with  $E_{\text{p}}^{\text{m}}$  values at  $-0.72$  V and  $-1.10$  V, also assigned to the reduction of the porphyrin ring to the  $\pi$ -radical anion and dianion forms. The reversible monoelectronic reduction peak observed at  $-1.31$  V and the irreversible peak at  $-1.64$  V correspond to the PEG chains. Zn<sup>II</sup>-3 also exhibited two irreversible monoelectronic anodic peaks at  $+1.61$  V and  $+1.80$  V, corresponding to the oxidation of the pyrrole groups to the radical cation and dication forms of the Zn porphyrin. This was followed by a multielectronic irreversible wave at  $+2.80$  V, corresponding to the degradation of the ether chains in the porphyrin. These data are in agreement

with the reported data for other perfluorinated Zn<sup>II</sup> porphyrins (Table S1†).<sup>68,69,79</sup> The Mn<sup>III</sup>-3 porphyrin exhibited a similar behaviour to that observed in aqueous media: at negative potentials two redox couples with  $E_p^m$  values at  $-0.828$  V and  $-1.131$  V, corresponding to porphyrin ring anion and dianion formation. These assignments were confirmed by a comparison with the data obtained for the free porphyrin, which show a trend in the potentials involving the reduction of the porphyrin moiety to be less negative for the free porphyrin than that in the Zn<sup>II</sup>-3 and Mn<sup>III</sup>-3 complexes, as also observed in HEPES buffer. The Mn<sup>II</sup>/Mn<sup>III</sup> core redox process in the Mn<sup>III</sup>-3 porphyrin was observed at  $E_p^m = +0.335$  V, with a peak separation  $\Delta E_p = 0.350$  V, again in agreement with the data for other perfluorinated Mn<sup>III</sup> porphyrins (Table S1†).<sup>68,69,79</sup> All the redox potentials obtained simultaneously in the two solvents were found to be lower in H<sub>2</sub>O than in DCE, in agreement with their relative dielectric constants and complexing abilities.

### Conversion between the Mn<sup>III</sup>-3 and Mn<sup>II</sup>-3 redox states

In order to evaluate the possibility of reduction of Mn<sup>III</sup>-3 to Mn<sup>II</sup>-3, two different biological reductants were used, ascorbic acid and BME. The reduction with ascorbic acid was followed by the study of UV-Vis spectra, recorded in PBS (phosphate buffer solution) under oxygen-free conditions in a argon deaerated solution of the Mn<sup>III</sup>-3 porphyrin upon addition of

increasing amounts of an argon deaerated solution of a reductant (Fig. 3a). Addition of 0.28 equivalents of ascorbic acid caused a decrease in the absorption at 457 nm (typical wavelength for the charge transfer Soret band (band V) of Mn<sup>III</sup> porphyrins), with the concomitant appearance of a new band at 434 nm, which is a typical absorption wavelength for Mn<sup>II</sup> porphyrins.<sup>80</sup> Total reduction of Mn<sup>III</sup>-3 to Mn<sup>II</sup>-3 was achieved after the addition of 25.3 equivalents of ascorbic acid. Conversely, oxidation of Mn<sup>II</sup>-3 to Mn<sup>III</sup>-3 was evaluated by acquiring the UV-Vis spectra of a deaerated Mn<sup>II</sup>-3 PBS solution, following exposure to air for 10 min, 4 h and 24 h (Fig. 3b). The system displays complete reversibility after 24 h. A similar study was performed with BME and complete reduction from Mn<sup>III</sup>-3 to Mn<sup>II</sup>-3 was achieved in the presence of 48 equivalents of this reductant (Fig. 3c). In this case, total reoxidation by air exposure was achieved after 72 h (Fig. 3d).

In contrast, reoxidation of Mn<sup>II</sup>-3 by the addition of an increasing number of equivalents of hydrogen peroxide showed no reversibility to Mn<sup>III</sup>-3 (Fig. S8†). Although the addition of up to the first equivalent gave mostly Mn<sup>III</sup>-3, further addition of a large excess led to the formation of Mn<sup>IV</sup> and Mn<sup>V</sup> oxo derivatives (Soret bands in the 424–443 nm region),<sup>72,73</sup> in agreement with the literature.<sup>80,81</sup>

Besides the quite different wavelengths of the Soret band, the UV-Vis spectra of Mn<sup>III</sup>-3 and Mn<sup>II</sup>-3 show other distinctive

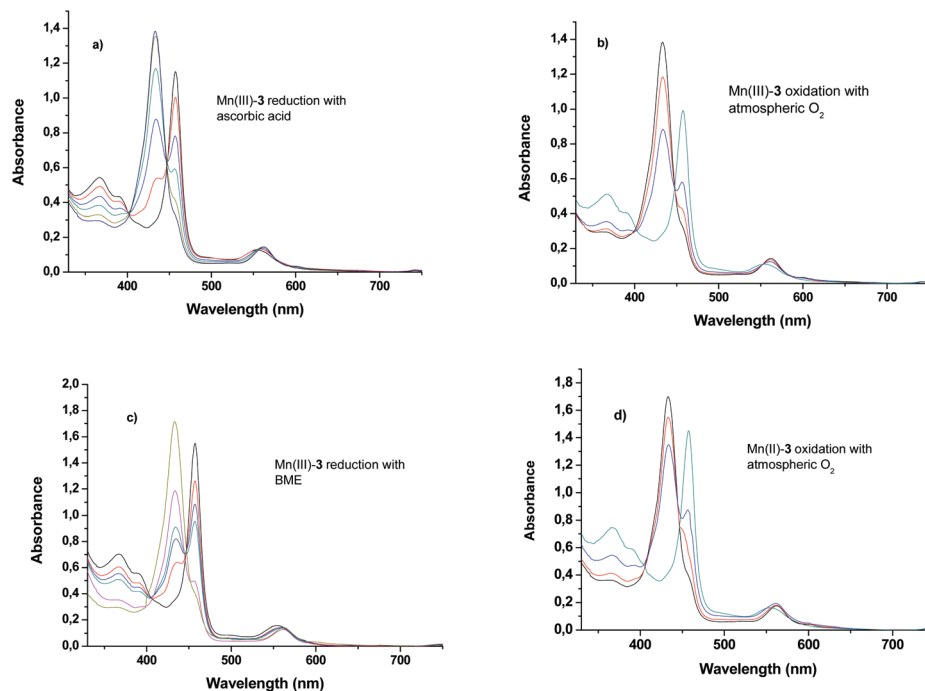


**Fig. 3** (a) UV-Vis reduction titration of 0.041 mM Mn<sup>III</sup>-3 with ascorbic acid, recorded in PBS (25 °C, pH = 7.4). Number of equivalents of ascorbic acid added: (black line) – 0; (red line) – 0.28; (light blue line) – 0.57; (light green line) – 0.85; (pink line) – 6.4; (dark green) – 11.4; (dark blue) – 25.3; (b) UV-Vis spectra of the reoxidation of Mn<sup>II</sup>-3 obtained (a) upon air exposure: (black line) – Mn<sup>II</sup>-3 before exposure; (red line) – after 10 min exposure; (blue line) – after 4 h exposure; (green line) – complete conversion to Mn<sup>III</sup>-3 (after 24 h exposure). (c) UV-Vis reduction titration of 0.041 mM Mn<sup>III</sup>-3 with BME, recorded in PBS (25 °C, pH = 7.4). Number of equivalents of BME added: (black line) – 0; (red line) – 0.43; (light blue line) – 2.32; (light green line) – 7.94; (pink line) – 23.5; (dark green) – 48; (d) UV-Vis spectra of the reoxidation of Mn<sup>II</sup>-3 obtained (c) upon air exposure: (black line) – Mn<sup>II</sup>-3 before exposure; (red line) – after 30 min exposure; (blue line) – after 24 h exposure; (green line) – complete conversion to Mn<sup>III</sup>-3 (after 72 h exposure).

differences (Fig. S9†). In the UV region, Mn<sup>III</sup>-3 shows two other bands, (VI and Va), less intense than the Soret band, at 367 and 391 nm, respectively, which in Mn<sup>II</sup>-3 decreases dramatically in intensity and shifts to 364 nm (VI), or disappears (Va). In the visible region, Mn<sup>III</sup>-3 displays a QIV band at 554 nm, which is shifted to 561 nm upon reduction, but the QIII band, usually observed in the 610–620 nm range, is not visible.<sup>67,75,80</sup> The absence of a decreased intensity of the Soret band and the absence of a band above 700 nm show that the porphyrin macrocycle is not reduced.<sup>82</sup>

In order to determine the empirical rate law for the reduction of Mn<sup>III</sup>-3 by ascorbic acid, a series of kinetic experiments were conducted at 25 °C (pH = 7.4) in the absence of oxygen and under pseudo-first order conditions, following the disappearance of the Soret band at 457 nm ( $\epsilon = 1.01 \times 10^4 \text{ M}^{-1} \text{ s}^{-1}$ ) over time at 50 ms intervals. Initial reaction rates were measured first at three different ascorbic acid concentrations (91, 191 and 390  $\mu\text{M}$ ) keeping the initial Mn<sup>III</sup>-3 concentration constant at 8  $\mu\text{M}$ , and then at three different initial Mn<sup>III</sup>-3 concentrations (95, 150 and 330  $\mu\text{M}$ ) in the presence of 9.8 mM ascorbic acid. The experimental data (Fig. S10 and S11†) evidenced that the reduction is first-order in relation to both Mn<sup>III</sup>-3 and ascorbic acid concentrations, with an overall second-order rate constant  $k_2 = 46.1 \pm 5.6 \text{ M}^{-1} \text{ s}^{-1}$ . Similar experiments with BME as the reductant yielded a  $k_2$  value of  $13.8 \pm 1.1 \text{ M}^{-1} \text{ s}^{-1}$ . These values are one to two orders of magnitude larger than the corresponding value of  $k_2 = 0.38 \text{ M}^{-1} \text{ s}^{-1}$  reported for the reduction of Mn<sup>III</sup>-HBET by glutathione.<sup>26</sup> The normal blood plasma concentration of ascorbic acid is in the 20–40  $\mu\text{M}$  range, which can be somewhat reduced in some pathologies, such as systemic inflammation.<sup>83,84</sup> For this ascorbic acid concentration range and in the absence of oxygen, the half-life of Mn<sup>III</sup>-3 is roughly 6–13 min. Ascorbic acid accumulates in circulating immune cells, such as neutrophils, monocytes and lymphocytes, reaching up to 1.2 to 3.5 mM concentrations.<sup>84</sup> In this range of concentrations, the half-life of Mn<sup>III</sup>-3 would be expected to decrease to about 4–12 s if it could enter those cells. Ascorbic acid, present in a neutral solution predominantly in the mono-anionic form ( $\text{HA}^-$ ), can be oxidized to dehydroascorbic acid, which appears in solution in the hydrate form Hy, with  $E_{\text{Hy}/\text{HA}}^{\circ'} = +0.184 \text{ V}$  in 0.1 M HEPES buffer at pH 7.4 (Fig. S7c†), which is slightly lower than the value +0.276 V reported in phosphate buffer.<sup>85</sup> This value is low enough to reduce the metal center of Mn<sup>III</sup>-3 ( $E_{\text{Mn(III)/Mn(II)}}^{\circ'} = +0.193 \text{ V}$ ) ( $K_{\text{eq}} \cong 1$  at 298 K) when present in excess, as that under our experimental conditions. BME is a non-natural thiol ( $E^{\circ'} = -0.26 \text{ V}$ )<sup>86</sup> also capable of reducing Mn<sup>III</sup>-3. A similar study with an aqueous solution of Mn<sup>III</sup>-TPPS<sub>4</sub> showed that no reduction occurred in the presence of ascorbic acid, which is in agreement with the reported redox potential of Mn<sup>III</sup>-TPPS<sub>4</sub> in aqueous solution ( $E_{\text{Mn(III)/Mn(II)}}^{\circ'} = -0.22 \text{ V}$ ).<sup>76</sup>

Reduction of Mn<sup>III</sup>-3 to Mn<sup>II</sup>-3 was not observed in the presence of glutathione even in a large excess of this important biological reductant. This is thermodynamically unexpected on the basis of their redox potentials, as the  $E^{\circ'}$  value

( $-0.240 \text{ V}$ )<sup>10</sup> of the GSSG/2GSH couple is negative enough to reduce Mn<sup>III</sup>-3, as observed with BME. In order to rationalize this finding, we compared the <sup>13</sup>C NMR spectrum of glutathione in the absence and in the presence of 0.1 equivalent of Mn<sup>III</sup>-3 in D<sub>2</sub>O (Fig. S12†). The addition of Mn<sup>III</sup>-3 causes the broadening of specific glutathione <sup>13</sup>C resonances: the two carboxylate peaks at 173.52 and 172.30 ppm ( $^- \text{O}-\text{C}=\text{O}$ ) and the signals of neighbouring carbon atoms at 53.58 ppm ( $^- \text{COO}-\text{C}-\text{NH}_2$ ) and 41.46 ( $^- \text{COO}-\text{C}-\text{NH}-$ ). This can be attributed to the binding of the terminal carboxylate groups of glutathione to the paramagnetic metal ion in the axial position of Mn<sup>III</sup>-3. Such binding mode is in agreement with X-ray crystal structures reported for complexes of Mn<sup>III</sup>-porphyrins with trichloroacetate.<sup>64</sup> On the other hand, we have shown above that electron transfer occurs with BME which has no carboxylate group. Altogether, this suggests that the coordination of glutathione to Mn<sup>III</sup>-3 to form a ternary complex blocks the electron transfer between the thiol group and the metal center and prevents the reduction. For the same reasons, reduction of Mn<sup>III</sup>-3 to Mn<sup>II</sup>-3 was also not observed, even in the presence of a large excess of cysteine (data not shown).

### Relaxivity studies

The relaxation properties were investigated for both the oxidized Mn<sup>III</sup> and the reduced Mn<sup>II</sup> forms of the porphyrin complex 3. Mn<sup>II</sup>-3 was obtained by adding 30 equivalents of ascorbic acid to the Mn<sup>III</sup> analogue. Full conversion of Mn<sup>III</sup>-3 to Mn<sup>II</sup>-3 was evidenced by recording UV-Vis spectra before the relaxivity measurements. The NMRD profiles recorded at 25 °C for the reduced and for the oxidized forms are presented in Fig. 4.

The reduction of the d<sup>4</sup> Mn<sup>III</sup>-3 complex to the electronically more symmetric d<sup>5</sup> Mn<sup>II</sup>-3 analogue leads to a large increase in the proton relaxivities at low and medium magnetic fields. Although a similar trend has been previously found for the Mn<sup>II</sup>/Mn<sup>III</sup>-TPPS<sub>4</sub> and Mn<sup>II</sup>/Mn<sup>III</sup>-TPPBr<sub>6</sub>S<sub>4</sub> analogues,<sup>62,87</sup> it was observable only in a much more restricted frequency range. Indeed, for these TPPS<sub>4</sub> analogues, the two curves cross each other at  $\sim 10 \text{ MHz}$ ,<sup>62</sup> while for our system, even at

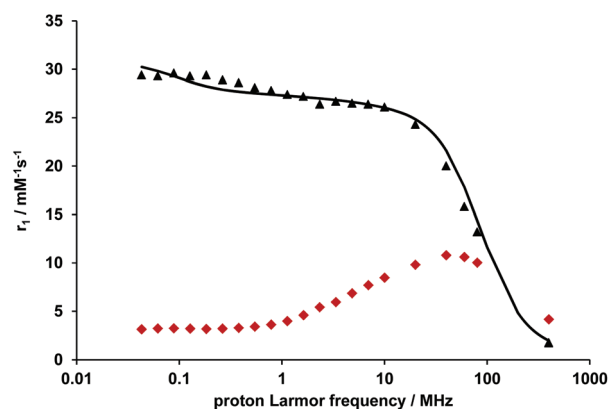


Fig. 4 Proton NMRD profiles recorded at 298 K for Mn<sup>III</sup>-3 (red  $\blacklozenge$ ) and Mn<sup>II</sup>-2 (black  $\blacksquare$ ). The curve represents the least squares fit to the data points as explained in the text.

80 MHz, the relaxivity of the reduced form remains ~30% higher than that of the oxidized form. In MR images, this would correspond to a remarkable “turn-on” response to a reducing environment.

As shown by Koenig<sup>34</sup> and later by Bryant,<sup>87</sup> attempts to fit the NMRD data for oxidized Mn<sup>III</sup>-TPPS<sub>4</sub> by using the Solomon–Bloembergen–Morgan theory do not yield satisfactory results for many of the fitted parameters. These include the distance between the Mn<sup>III</sup> ion and the protons of the coordinated water molecules,  $r_{\text{MnH}}$ , which showed highly temperature-dependent values ranging from 2.13 Å (35 °C) to 2.48 Å (5 °C), which is way too short in light of the structural data available from X-ray crystallographic studies.<sup>88</sup> They also used a value for the water exchange rate,  $k_{\text{ex}}^{298} = 10^9 \text{ s}^{-1}$ , which is too large when compared with the  $k_{\text{ex}}^{298}$  values of  $14 \times 10^6 \text{ s}^{-1}$  and  $27.4 \times 10^6 \text{ s}^{-1}$  determined from the temperature dependence of <sup>17</sup>O NMR relaxation times.<sup>89,90</sup> It was indeed evidenced that the relaxation mechanism of Mn<sup>III</sup> porphyrin derivatives has unique aspects, the most important being the unusual role of ZFS interactions and the effect of these interactions on the electron spin dynamics.<sup>35</sup> Consequently, the analysis of the NMRD curves of Mn<sup>III</sup>-3 requires a complex mathematical treatment which, in the case of Mn<sup>III</sup>-TPPS<sub>4</sub>, gave a reasonable and temperature-independent  $r_{\text{MnH}}$  value of 2.80 Å. Values for other parameters were also calculated. At 20 °C values of the rotational correlation time,  $\tau_{\text{R}} = 900 \text{ ps}$ , and two different electron spin relaxation times  $\tau_{\text{S}}^{(\pm 1)} = 506 \text{ ps}$  and  $\tau_{\text{S}}^{(\pm 2)} = 180 \text{ ps}$  for the  $M_{\text{S}} = \pm 1$  and  $\pm 2$  non-Kramers manifolds, respectively, were reported.<sup>35</sup> When compared with the corresponding calculated SBM parameters,<sup>87</sup>  $\tau_{\text{R}} = 275 \text{ ps}$ , and the parameters describing the electron spin relaxation, the correlation time for the modulation of the zero-field-splitting,  $\tau_{\text{v}} = 30 \text{ ps}$ , and the electron spin relaxation time at zero magnetic field,  $\tau_{\text{SO}} = 15 \text{ ps}$ , one concludes that the SBM treatment underestimated  $\tau_{\text{R}}$  and  $\tau_{\text{SO}}$  and gave a very high  $\tau_{\text{v}}$  value. However, such a mathematical treatment for the analysis of the NMRD curves of Mn<sup>III</sup>-3 is beyond the scope of the present work. Despite this, our observation that the  $r_1$  values of Mn(III)-3 at low fields are systematically lower than those of Mn<sup>III</sup>-TPPS<sub>4</sub><sup>62,87</sup> can be qualitatively explained from their relative electronic relaxation parameters, which dominate  $r_1$  at such fields. Thus, we can say that Mn(III)-3 shows faster electronic relaxation than Mn<sup>III</sup>-TPPS<sub>4</sub> as a result of the fluorinated phenyl substituents at the porphyrin *meso* positions.

Concerning the Mn<sup>II</sup>-3 complex, its NMRD curve was analysed within the frame of the SBM theory (see the ESI† for equations). The outer sphere relaxation contribution was considered according to the translational diffusion model developed by Freed.<sup>91</sup> There are a large number of parameters that appear in the analysis and some of them have been fixed to reasonable values. These involve the distance between the Mn<sup>II</sup> electron spin and the proton of the coordinated water molecules ( $r_{\text{MnH}} = 3.1 \text{ Å}$ ), the distance of the closest approach of water protons diffusing around the complex which determines the outer sphere interactions ( $a_{\text{MnH}} = 3.6 \text{ Å}$ ) and the relative translational diffusion coefficient ( $D_{\text{MnH}} = 26 \times 10^{-10} \text{ m}^2 \text{ s}^{-1}$ ). The hydration number was also fixed to  $q = 2$ , in analogy to the TPPS<sub>4</sub> analogue. In the fit, we adjusted the rotational correlation time,  $\tau_{\text{R}}$ , the parameters describing electron spin relaxation,  $\tau_{\text{v}}$ , the correlation time for the modulation of the zero-field-splitting and  $\Delta^2$ , the energy of the zero-field-splitting. The water exchange rate could not be measured for Mn<sup>II</sup>-3 by variable temperature <sup>17</sup>O NMR, as it is typically done for paramagnetic complexes, due to solubility problems at higher temperatures. Therefore, we also adjusted this parameter. The fit is rather satisfactory (Fig. 4) and the resulting parameters are shown in Table 1, in comparison with some other Mn<sup>II</sup> complexes. We should note that the inclusion of a scalar relaxation mechanism into the fit by assuming a scalar coupling constant of  $A_{\text{h}} = 0.5 \text{ MHz}$  did not improve the quality of the fit and did not have an important effect on the other fitted parameters.

Bryant *et al.* reported some time ago on the analysis of the NMRD profile of Mn<sup>II</sup>TPPS<sub>4</sub>.<sup>87</sup> They concluded that it was impossible to describe the Mn<sup>II</sup>TPPS<sub>4</sub> system using the SBM theory and with a reasonable set of parameters. In their best fit, they used a reasonable  $k_{\text{ex}}^{298} = 10^7 \text{ s}^{-1}$ ,  $\tau_{\text{R}}^{298} = 300 \text{ ps}$  and a very short  $\tau_{\text{v}}^{298} = 0.5 \text{ ps}$ . The outer sphere contribution was parameterized with a very short distance for the closest approach of water protons to the manganese center ( $a_{\text{MnH}} = 2.0 \text{ Å}$ ) and a very small value for the diffusion constant ( $6 \times 10^{-10} \text{ m}^2 \text{ s}^{-1}$ ). To explain these discrepancies, they proposed that the dipole–dipole approximation of the SBM theory might fail for these porphyrin complexes which can undergo an electron spin delocalization from the manganese ion to the porphyrin. This hypothesis seemed to be supported by the fact that a derivative, Mn<sup>II</sup>-TPPBr<sub>6</sub>S<sub>4</sub>, which was brominated on the pyrrole rings, had even higher proton relaxivities. In our ana-

**Table 1** Relaxivities and fitted parameters for Mn<sup>II</sup>-3 and other Mn<sup>II</sup> complexes from the literature

Parameter	Mn <sup>II</sup> -3	[Mn(15-py N <sub>3</sub> O <sub>2</sub> )(H <sub>2</sub> O) <sub>2</sub> ] <sup>2+</sup> 92	[Mn(H <sub>2</sub> O) <sub>6</sub> ] <sup>2+</sup> 93
$r_1/\text{mM}^{-1} \text{ s}^{-1}$ 20 MHz/298 K	24.3	4.48	7.4 <sup>a</sup>
$k_{\text{ex}}^{298}/10^6 \text{ s}^{-1}$	0.81 ± 0.2	3.8	21
$\tau_{\text{RH}}^{298}/\text{ps}$	4800 ± 1000	40.3	30 <sup>b</sup>
$\tau_{\text{v}}^{298}/\text{ps}$	5 ± 1	3.3	3.3
$\Delta^2/10^{18} \text{ s}^{-2}$	0.50 ± 0.2	6.6	5.6

<sup>a</sup> This work. <sup>b</sup> 308 K.<sup>94</sup>



lysis, the  $\text{Mn}^{\text{II}}$ -proton distances and the diffusion constant have values typical of  $\text{Mn}^{\text{II}}$  chelates. The water exchange rate is also reasonable. The rotational correlation time has a high value, but it is not surprising given the presence of four PEG chains attached to the porphyrin ring. The fact that the paramagnetic metal is in the barycenter of a large molecule implies that it takes full benefit from the slow rotation of the whole molecule. A porphyrin center bearing four  $\text{Gd}^{\text{III}}$  complexes, with a similar molecular weight ( $M_w = 2.76$  kDa), thus the molecular size, to that of  $\text{Mn}^{\text{II}}$ -3 ( $M_w = 2.99$  kDa) has been recently reported.<sup>95</sup> Here the paramagnetic  $\text{Gd}^{\text{III}}$  complexes are not in the barycenter of the molecule. However, the relaxivities were analyzed with the Lipari-Szabo approach that allows calculating the global rotational correlation time,  $\tau_g$ , which can then be related to the rotational motion of the entire molecule. The global rotational correlation time for this tetra-Gd porphyrin was found to be  $\tau_g = 2.3$  ns, similar in the nanosecond range to the  $\tau_R$  calculated for  $\text{Mn}^{\text{II}}$ -3. This gives confidence in the fit of the NMRD profile for  $\text{Mn}^{\text{II}}$ -3. Even if the errors on the calculated parameters are higher than usual given the lack of independent determination for the water exchange rate, their order of magnitude should be correct.

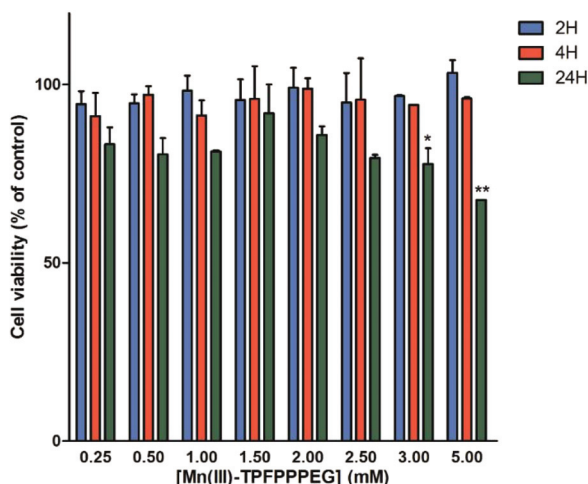


**Fig. 5** Effect of increasing concentrations of the  $\text{Mn}^{\text{III}}$ -3 porphyrin compound on HeLa cell viability as a function of time. HeLa cells were plated in 96-well plates at a density of  $2 \times 10^4$  cells per well. Twenty-four hours after plating, the cells were incubated with 0.25, 0.5, 1.0, 1.5, 2.0, 2.5, 3.0 and 5.0 mM solutions of  $\text{Mn}^{\text{III}}$ -3. Cell viability was measured after 2, 4 or 24 h using the Alamar Blue assay. Cell viability is presented relative to the percentage of untreated cells (control cells) considered as 100%. Data represent the mean  $\pm$  SD of three independent experiments. Pairwise data comparisons were performed between cell viability values obtained with each  $\text{Mn}^{\text{III}}$ -3 concentration, as compared with the immediately precedent concentration, for each incubation period (non-significant) and between cell viability values obtained for each incubation period with  $\text{Mn}^{\text{III}}$ -3, as compared with the immediately precedent incubation period, for each concentration (\*\* $p < 0.01$ , \* $p < 0.05$ ). The significance of the results was statistically analyzed by one-way analysis of variance (ANOVA) with Tukey's multiple pairwise comparison. Statistical significance was set at  $p < 0.05$ .

## Evaluation of the cytotoxicity of $\text{Mn}^{\text{III}}$ -3 in a cell model

The *in vitro* cytotoxicity of  $\text{Mn}^{\text{III}}$ -3 on the epithelial HeLa tumor cell line was evaluated using the Alamar Blue colorimetric assay. The cells were incubated with solutions containing different concentrations of  $\text{Mn}^{\text{III}}$ -3 (0.25–5 mM), prepared from a PBS stock solution and diluted in DMEM complete medium, during different time periods (2 h, 4 h and 24 h). The  $\text{Mn}^{\text{III}}$ -3 compound was soluble in aqueous solution and the tested concentrations were in the meaningful range for the desired biomedical application.

As shown in Fig. 5, no statistically significant toxicity was observed after 2 and 4 h of incubation for all the concentrations used. After 24 h exposure to the compound, a statistically significant decrease in cell viability was observed for the highest concentrations tested (3 and 5 mM). In addition to its water solubility, the absence of statistically significant cytotoxicity of  $\text{Mn}^{\text{III}}$ -3 in the concentration and exposure time ranges normally used in *in vivo* MRI, are positive indications of its potential application as a redox-responsive agent (Fig. 5).

## Conclusions

A new water-soluble fluorinated porphyrin derivative conjugated with PEG chains was synthesized. It is capable of stabilizing both  $\text{Mn}^{\text{III}}$  and  $\text{Mn}^{\text{II}}$  oxidation states in a biologically relevant range of redox potentials. In aqueous solution,  $\text{Mn}^{\text{III/II}}$ -3 undergoes reversible reduction/oxidation reactions, promoted by the natural reducing agent ascorbic acid and oxygen, respectively. In the absence of oxygen, the reduction process with ascorbic acid shows second-order kinetics, with a  $k_2$  value of  $46.1 \text{ M}^{-1} \text{ s}^{-1}$ , which is two orders of magnitude larger than the  $k_2$  of  $0.38 \text{ M}^{-1} \text{ s}^{-1}$  reported for the reduction of  $\text{Mn}^{\text{III}}$ -HBET by glutathione.<sup>26</sup> This corresponds, in the absence of oxygen, to a half-life of a few minutes in blood plasma and a few seconds in circulating immune cells where ascorbic acid reaches 20–40  $\mu\text{M}$  and a few mM concentrations, respectively. Re-oxidation by air oxygen ( $p\text{O}_2 = 160$  mmHg) is quite slow but it is fully achieved after 24 h. However, the above half-lives are expected to be longer in different *in vivo* environments, with widely varying oxygen levels, but usually in a larger excess than ascorbic acid. Oxygen levels are high in arterial blood ( $p\text{O}_2 = 100$  mmHg) while lower in venous blood ( $p\text{O}_2 = 40$  mmHg) as well as in different tissues, depending on their vascular architecture and oxygen demand. The  $p\text{O}_2$  is quite low (<10–15 mmHg) under hypoxic conditions, such as in non-necrotic tumour tissue, and even lower ( $p\text{O}_2 < 2$ –3 mmHg) in necrotic tumour cores.  $\text{Mn}^{\text{III}}$ -3 reduction by an ascorbate is complete within minutes, while reoxidation by oxygen is slow but is dependent on highly varying tissue oxygenation levels. Consequently, the *in vivo* kinetics of the MRI signal variation of  $\text{Mn}^{\text{II}}$ / $\text{Mn}^{\text{III}}$ -3 is expected to be quite sensitive to the oxygenation state of tissues, in particular under hypoxic or anoxic conditions.

Interestingly,  $^{19}\text{F}$  NMR resonances of  $\text{Mn}^{\text{III}}$ -3 are relatively sharp which could open further possibilities to exploit such complexes as paramagnetic  $^{19}\text{F}$  NMR probes.<sup>96</sup>

At medium frequencies (20–80 MHz), the relaxivity increase between the Mn<sup>III</sup>-3 and Mn<sup>II</sup>-3 complexes is considerably improved with respect to the previously studied Mn-TPPS<sub>4</sub> analogue<sup>62</sup> (at 40 MHz,  $\Delta r_1 \sim 100\%$ ). Cytotoxicity evaluation on epithelial HeLa cells confirmed *in vitro* non-toxicity of the compound in the mM concentration range typically used for MR imaging.

In general, the development of MRI imaging probes to monitor redox environments *in vivo* faces several difficulties. Mn<sup>II/III</sup> chelates of open-chain hydroxybenzyl-ethylenediamine acetic acid derivatives have been reported to possess favorable *in vitro* properties as redox active MRI contrast agents,<sup>30</sup> but their kinetic stability might be insufficient. In this respect, Mn-porphyrin redox responsive probes can be advantageous.

The present Mn<sup>II</sup>/Mn<sup>III</sup>-porphyrin couple satisfies many of the criteria required for a redox imaging probe: good water solubility, biocompatibility, non-toxicity, thermodynamic and kinetic stability in both metal oxidation states, a redox half-cell potential accessible to biologically relevant reducing agents with fast kinetics (adapted to the imaging time scale), and a strong “turn on” relaxivity response upon reduction. However, it is not reduced by glutathione or cysteine, the major thiol-disulfide redox buffers of the intracellular and extracellular spaces, respectively. In human plasma, cysteine–cystine and glutathione reach levels of  $\sim 260$  microM and  $\sim 7$  microM, respectively,<sup>97</sup> while ascorbic acid has a 20–40 microM concentration.<sup>83,84</sup> Therefore, the role of ascorbic acid should not be ignored in maintaining the extracellular redox state. Our redox sensitive MRI probe might have the potential to report, with fast kinetics (few minutes half-life), on the extracellular ascorbate without the interference of the cysteine–cystine buffer. In circulating immune cells for instance, ascorbic acid amounts to millimolar concentrations and controls the redox state. Provided the probe is modified for cell internalization to reach mM concentrations, it could be useful to assess intracellular ascorbic acid in such cells with very fast kinetics (few seconds half-life).

Furthermore, MRI quantification of ascorbate could also be achieved by separating the effect of the *in vivo* concentration of the probe from the redox effect on the observed contrast. For this, a ratiometric technique could be used,<sup>98</sup> based on injecting a cocktail of the <sup>52</sup>Mn-radiolabeled porphyrin and the normal one. Indeed, <sup>52</sup>Mn ( $t_{1/2} = 5.59$  d,  $\beta^+ = 29.6\%$ ,  $E_{\beta\text{ave}} = 0.24$  MeV) is a promising positron emission tomography (PET) radioisotope,<sup>99</sup> which allows the direct combination of PET and MRI detection. The advantage of this technique is the identical biodistribution of the PET and MRI probes. As PET is a quantitative technique, it will allow assessing the concentration of the MRI probe as well, leading to quantification of the ascorbate concentration.

## Experimental section

### Materials and methods

Commercially available reagents were bought from Aldrich, except PEG500 (mono-methyl polyethyleneglycol) (Fluorochem

and used as received. All solvents were pre-dried according to standard laboratory techniques. For the cyclic voltammetry experiments, 1,2-dichloroethane (DCE) was purchased with the highest quality available, and stored in molecular sieves, under an inert atmosphere. The other reagents were also purchased with the highest quality available and were used as received. 5,10,15,20-(Pentafluorophenyl)porphyrin was synthesized according to the literature.<sup>64</sup> UV-visible absorption spectra were recorded on a Hitachi U-2010 using quartz cells. The molar absorption coefficients were determined using PBS as the solvent. <sup>1</sup>H-NMR and <sup>19</sup>F-NMR spectra were recorded on a 400 MHz Bruker Avance III NMR spectrometer (400.101 and 376.5 MHz, respectively). Proton chemical shifts are given in parts per million (ppm) relative to tetramethylsilane at  $\delta$  0.00 ppm and <sup>19</sup>F relative to TFA at  $\delta$  –76.55 ppm. Mass spectra (ESI-FIA-TOF) were acquired using an Applied Biosystems Voyager DE-STR instrument equipped with a nitrogen laser ( $\lambda = 337$  nm).

### Synthesis

**5,10,15,20-(4-PEG500-2,3,5,6-fluorophenyl)porphyrin (TPFPP (PEG)<sub>4</sub>, 2).** A mixture of 5,10,15,20-(pentafluorophenyl)porphyrin (140 mg, 0.14 mmol) and PEG500 (mono-methyl polyethyleneglycol –  $M_w = \sim 500$  Da) (0.359 mL, 0.718 mmol) was dissolved in 10 mL of dry DMF. After the addition of NaH (17 mg, 0.718 mmol) the reaction mixture was left at room temperature, until complete consumption of 5,10,15,20-(pentafluorophenyl)porphyrin, monitored by TLC (2 hours). The reaction mixture was extracted several times with dichloromethane/water and dichloromethane/aqueous 1 M K<sub>2</sub>CO<sub>3</sub> and the organic layer was dried over anhydrous sodium sulfate and concentrated under vacuum. Porphyrin 2 was obtained in 78% yield. <sup>1</sup>H NMR (400 MHz, CDCl<sub>3</sub>)  $\delta$ , ppm: 8.93 (s, 8 H<sub>B</sub>), 3.65–3.60 (m, 160–196 (polydisperse distribution) H<sub>PEG</sub>), –2.90 (s, 2 H<sub>NH</sub>); <sup>19</sup>F NMR (376 MHz, CDCl<sub>3</sub>)  $\delta$ , ppm: –138.86–(–138.04) (m, 4F), –157.97–(–157.03) (m, 4F). MS (ESI-FIA-TOF)  $m/z$ : 1028.3720, 1220.9980, 1287.0377, 1491.1818 [M]<sup>2+</sup> (polydisperse distribution).

**Mn<sup>III</sup>-5,10,15,20-(4-PEG500-2,3,5,6-fluorophenyl)porphyrin (Mn<sup>III</sup>-TPFPP(PEG)<sub>4</sub>, Mn<sup>III</sup>-3).** Free base 2 (100 mg, 0.045 mmol), sodium acetate (367 mg, 4.47 mmol) and manganese(II) acetate were dissolved in 3 mL of acetic acid. The reaction mixture was stirred at 80 °C and controlled by UV-Vis spectroscopy. After complete conversion to the manganese complex (2 hours), the reaction mixture was extracted several times with dichloromethane/water and then the organic layer was dried over anhydrous sodium sulfate and concentrated under vacuum. Porphyrin 3 was obtained in 85% yield. MS (ESI-FIA-TOF)  $m/z$ : 1121.3612, 1319.9802, 1386.0195, 1493.6057 [M]<sup>2+</sup> (polydisperse distribution).

**Zn<sup>II</sup>-5,10,15,20-(4-PEG500-2,3,5,6-fluorophenyl)porphyrin (Zn<sup>II</sup>-TPFPP(PEG)<sub>4</sub>, Zn<sup>II</sup>-3).** Free base 2 was dissolved in a mixture of chloroform/methanol (2 : 1) and zinc(II) acetate was added. The reaction mixture was stirred at 50 °C and controlled by UV-Vis spectroscopy. After complete conversion (1 h) the reaction mixture was extracted several times with dichloro-

methane/water and the organic phase was dried over anhydrous sodium sulfate and concentrated under vacuum. The zinc derivative was obtained in 89% yield.  $^1\text{H}$  NMR (400 MHz,  $\text{CDCl}_3$ )  $\delta$ , ppm: 8.88 (s, 8  $\text{H}_\beta$ ), 3.67–3.12 (m, 160–196 (polydisperse distribution)  $\text{H}_{\text{PEG}}$ ). MS (ESI-FIA-TOF)  $m/z$ : 1445.0650, 1467.0780, 1489.0912, 1511.1044  $[\text{M}]^{2+}$  (polydisperse distribution).

**$\text{Mn}^{\text{III}}$ -5,10,15,20-tetrakis(4-sulfonatophenyl)porphyrin ( $\text{Mn}^{\text{III}}$ TPPS<sub>4</sub>).** TPPS<sub>4</sub> was synthesized according to the literature.<sup>100</sup>  $\text{Mn}^{\text{III}}$ TPPS<sub>4</sub> was obtained using the same procedure used for porphyrin  $\text{Mn}^{\text{III}}$ -3. Characterization is performed in accordance with the literature.<sup>67</sup>

### Electron paramagnetic resonance (EPR)

X-band (0.34 T, 9.5 GHz) continuous wave (CW) EPR measurements were carried out on a Bruker EMX spectrometer, equipped with a continuous flow Oxford Instruments cryostat for low temperature measurements. The EPR experiments were performed on the  $\text{Mn}^{\text{II}}$  salt  $\text{MnCl}_2$  and  $\text{Mn}^{\text{III}}$ -porphyrin samples in aqueous solution at 25 °C (see the ESI†). Simulation of the experimental spectra of aqueous  $\text{Mn}^{2+}$  was performed using SimFonia v.1.2 (Bruker Instruments Inc. software). The EPR spectra showed that the residual  $\text{Mn}^{2+}$  aqueous ion concentrations present in the  $\text{Mn}^{\text{III}}$ -porphyrin solutions used for the NMRD measurements were lower than 10  $\mu\text{M}$ .

### $^1\text{H}$ relaxometry

The longitudinal ( $T_1$ ) proton relaxation times of aqueous solutions of the  $\text{Mn}^{\text{III}}$  and  $\text{Mn}^{\text{II}}$  complexes were measured at 25 °C and 37 °C by nuclear magnetic resonance relaxometry on a Bruker Minispec mq20 relaxometer operating at a magnetic field of 0.47 T, corresponding to a proton Larmor frequency of 20 MHz, using an inversion recovery pulse sequence. All the experimental values were corrected taking into account the diamagnetic contribution of water. The corresponding relaxivity values ( $r_1$ ) were calculated through the least-squares curve fitting of the inverse relaxation time  $1/T_1$  ( $\text{s}^{-1}$ ) vs. the  $\text{Mn}^{\text{II/III}}$  concentration.  $^1\text{H}$  NMRD (Nuclear Magnetic Relaxation Dispersion) profiles were recorded on a Stelar SMARtracner Fast Field Cycling NMR relaxometer (0.01–10 MHz) and a Bruker WP80 NMR electromagnet (20, 40, 60 and 80 MHz) adapted to variable field measurements and controlled by a SMARtracner PC-NMR console. The temperature was monitored with a VTC91 temperature control unit and maintained by a gas flow. The temperature was determined by previous calibration with a Pt resistance temperature probe. The longitudinal relaxation rates ( $1/T_1$ ) were determined in water at 25 °C and 37 °C. High field relaxivities were measured on a Bruker AVANCE NMR spectrometer at 400 MHz by placing the sample solution in an inner co-axial tube while the outer tube was filled with  $\text{D}_2\text{O}$ .

### Reduction kinetics

To  $1.35 \times 10^{-5}$  M stock solutions of  $\text{Mn}^{\text{III}}$ -3 in PBS (25 °C, pH = 7.4) were added appropriate volumes of 50 mM ascorbic acid or of 63 mM BME. For one set of experiments, the final concentration of  $\text{Mn}^{\text{III}}$ -3 was kept at 0.008 mM and those of ascorbic acid were 0.390 mM, 0.191 mM and 0.091 mM. For

the other set, the final concentration of ascorbic acid was constant at 9.7 mM and those of  $\text{Mn}^{\text{III}}$ -3 were 0.230 mM, 0.150 mM and 0.095 mM. The same final concentrations were used for the BME experiments.

The conversion of  $\text{Mn}^{\text{III}}$ -3 to  $\text{Mn}^{\text{II}}$ -3 was monitored by the disappearance of a strong UV-Vis absorbance at 457 nm ( $\epsilon = 1.01 \times 10^4 \text{ M}^{-1} \text{ s}^{-1}$ ) which is absent in the UV-vis spectrum of the  $\text{Mn}^{\text{II}}$ -3 complex. The decrease of the absorbance at 457 nm of  $\text{Mn}^{\text{III}}$ -3 in the presence of excess ascorbic acid or BME, with the concomitant appearance of a new band characteristic of the  $\text{Mn}^{\text{II}}$ -3 spectrum, was monitored over time. All the solutions used were argon deaerated and measured in a sealed cuvette. The experimental setup used to monitor the kinetics of the reaction consisted of a fiber coupled Ocean Optics spectrometer (USB4000-UV-Vis) used in absorption mode together with a MiKropack DH-2000-BAL UV-Vis-NIR light source. The absorption spectra were recorded at intervals of 50 ms (for ascorbic acid) and 100 ms (for BME) and monitored up to the complete formation of the  $\text{Mn}^{\text{II}}$ -3 species. The large excess of ascorbic acid and of BME used in the experiments ensured pseudo-first-order kinetics with respect to the  $\text{Mn}^{\text{III}}$ -3 complex as expressed in eqn (1):

$$\ln[\text{Mn}^{\text{III}}\text{-3}]_t = -k_{\text{obs}}t + \ln[\text{Mn}^{\text{III}}\text{-3}]_0 \quad (1)$$

Here,  $k_{\text{obs}}$  refers to the observed pseudo-first-order rate constant, which is the product of the actual rate constant ( $k$ ) and  $[\text{ascorbic acid}]_0$ ,  $t$  is the time and the subscripts “ $t$ ” and “0” correspond to the calculated concentration at time “ $t$ ” and the initial concentration, respectively.

### Cyclic voltammetry

The electrochemical experiments in aqueous solutions were carried out using 0.1 M HEPES buffer, pH 7.4, prepared from *N*-[2-hydroxyethyl]piperazine-*N'*-[2-ethanesulfonic acid] hemisodium salt (Sigma, St Louis, USA), as a supporting electrolyte. The porphyrin stock solutions were prepared by dissolving the solid compounds in HEPES buffer, followed by further dilution in buffer when needed. Millipore Milli-Q nanopure water (resistivity  $\geq 18 \text{ M}\Omega \text{ cm}$ ) was used for the preparation of all solutions. All experiments were performed at room temperature ( $25 \pm 1$  °C). The pH measurements were carried out with a CRISON 2001 micro pH-meter (Crison, Spain). Cyclic voltammetry (CV) measurements were carried out with an Autolab PGSTAT-30 potentiostat/galvanostat (Eco Chemie, Utrecht, Netherlands), controlled by the GPES 4.9 software. The electrochemical cell, with a 2 mL volume, contained a glassy carbon electrode ( $d = 1 \text{ mm}$ ) as the working electrode, a platinum wire as the counter electrode and Ag/AgCl (3 M KCl) as the reference electrode. Prior to the CV measurements, all solutions were degassed by  $\text{N}_2$  bubbling for 15 min and during potential cycling a flux of  $\text{N}_2$  was kept flowing on top of the cell solution.

Some CV measurements were also carried out in DCE solutions in the presence of 0.6 M  $\text{Bu}_4\text{NBF}_4$ . These were performed using a homemade potentiostat.<sup>101</sup> A jacketed five neck conical cell was used. Three of the necks were used for the



working, counter, and reference electrodes, while the other two necks were used for the argon inlet and outlet. A glassy carbon disk with a 1 mm diameter was used as the working electrode, with the counter electrode being a 1 mm diameter Pt disk. The reference electrode was a saturated calomel electrode (SCE), separated from the working electrode compartment by a salt bridge with a ceramic frit. Experiments were performed at 10 °C, using a HAAKE F3 circulation system in order to avoid the DCE solvent evaporation. Electrochemical characterisation of ferrocene was used as an electrochemical standard in DCE. Ferrocene showed a one-electron transfer. The current values were standardised with respect to the concentration and scan rate square-root, in order to determine the number of electrons associated with an unknown electronic transfer.

All the potentials obtained were corrected to be reported referenced to the normal hydrogen electrode (NHE).

### Cytotoxicity studies

HeLa cells (human epithelial cervical carcinoma cell line) were maintained at 37 °C under an O<sub>2</sub>/CO<sub>2</sub> (95%/5%) atmosphere in Dulbecco's modified Eagle's medium (DMEM, Sigma, St Louis, MO), supplemented with heat-inactivated fetal bovine serum (10% (v/v), FBS, Sigma), penicillin (100 U mL<sup>-1</sup>) and streptomycin (100 µg mL<sup>-1</sup>). HeLa cells grown in a monolayer were detached by treatment with trypsin solution (0.25%, Sigma) and were seeded in medium (2 × 10<sup>4</sup> cells per mL (100 µL per well)) in 96-well culture plates. After 24 h, when the cells were at 50–70% confluence, they were incubated with the compound to be tested. The cytotoxicity induced by the compound in HeLa cells was evaluated using the modified Alamar Blue colorimetric assay, as previously described.<sup>102</sup> Briefly, a stock solution of the compound under study was prepared in phosphate buffer saline (PBS), and successive dilutions in DMEM complete medium were prepared from this stock in order to achieve the concentration range of 0.25 mM to 5 mM. The diluted solutions were added to the cells 24 h after seeding, followed by incubation of the cultures at 37 °C for 2, 4, and 24 h. For each time point, 0.1 mL of a resazurin dye solution (1% (v/v), Sigma) in DMEM medium was added to each well. After 45 min of incubation at 37 °C, the absorbance was measured at 570 and 600 nm with a SPECTRAMax PLUS 384 spectrophotometer (Molecular Devices, Union City, CA). Although the compound under study is colored, its maximum absorbance is at λ ≈ 460 nm and at λ ≈ 440 nm, respectively, for the oxidized and the reduced forms (Fig. 3 and Fig. S6<sup>†</sup>), thus not interfering with the results obtained from the Alamar Blue assay.

For each concentration of the compound, the percentage of cell viability was calculated according to eqn (2):

$$\% \text{ cell viability} = \frac{[(A_{570} - A_{600})_{\text{treated cells}}]}{[(A_{570} - A_{600})_{\text{control cells}}]} \times 100 \quad (2)$$

where the control cells (control +) refer to cells not exposed to the compound, corresponding to 100% cell viability. It was also considered a negative control (control -) of the resazurin

dye solution and the respective absorbance was subtracted from the values measured in all the samples.

Statistical analysis was carried out using one-way ANOVA with Tukey's multiple pairwise comparison. A value of  $p < 0.05$  was considered as statistically significant.

## Conflicts of interest

There are no conflicts to declare.

## Acknowledgements

The authors thank the joint France (ANR)-Portugal (FCT) PESSOA 3750-37687RE project, FCT-Portugal (Portuguese Foundation for Science and Technology) and FEDER – European Regional Development Fund through the COMPETE Programme (Operational Programme for Competitiveness) for funding with UID/QUI/00313/2019 and POCI-01-0145-FEDER-027996. S. M. A. P., M. J. F. C., M. E. G. and A. M. S. C. are grateful for the SFRH/BPD/84619/2012, SFRH/BPD/99698/2014, SFRH/BPD/103103/2014 and SFRH/BPD/99613/2014 post-doctoral grants, respectively. E. T. is grateful to the Ligue contre le Cancer (France) for their financial support.

## Notes and references

- 1 D. Trachootham, W. Q. Lu, M. A. Ogasawara, N. R. D. Valle and P. Huang, *Antioxid. Redox Signaling*, 2008, **10**, 1343–1374.
- 2 D. F. Quail and J. A. Joyce, *Nat. Med.*, 2013, **19**, 1423–1437.
- 3 N. W. Lutz, Y. Le Fur, J. Chiche, J. Pouyssegur and P. J. Cozzone, *Cancer Res.*, 2013, **73**, 4616–4628.
- 4 A. Rubartelli and M. T. Lotze, *Trends Immunol.*, 2007, **28**, 429–436.
- 5 E. H. Sarsour, M. G. Kumar, L. Chaudhuri, A. L. Kalen and P. C. Goswami, *Antioxid. Redox Signaling*, 2009, **11**, 2985–3011.
- 6 D. J. Hausenloy and D. M. Yellon, *J. Clin. Invest.*, 2013, **123**, 92–100.
- 7 T. C. Jorgenson, W. X. Zhong and T. D. Oberley, *Cancer Res.*, 2013, **73**, 6118–6123.
- 8 R. Banerjee, *J. Biol. Chem.*, 2012, **287**, 4397–4402.
- 9 L. Chaiswing and T. D. Oberley, *Antioxid. Redox Signaling*, 2010, **13**, 449–465.
- 10 F. Q. Schafer and G. R. Buettner, *Free Radical Biol. Med.*, 2001, **30**, 1191–1212.
- 11 C. Vandeputte, I. Guizon, I. Genestiedenis, B. Vannier and G. Lorenzon, *Cell Biol. Toxicol.*, 1994, **10**, 415–421.
- 12 I. Rahman, A. Kode and S. K. Biswas, *Nat. Protoc.*, 2006, **1**, 3159–3165.
- 13 L. M. De Leon-Rodriguez, A. J. M. Lubag, C. R. Malloy, G. V. Martinez, R. J. Gillies and A. D. Sherry, *Acc. Chem. Res.*, 2009, **42**, 948–957.



- 14 E. M. Gale, S. Mukherjee, C. Liu, G. S. Loving and P. Caravan, *Inorg. Chem.*, 2014, **53**, 10748–10761.
- 15 M. Bourgeois, H. Rajerison, F. Guerard, M. Mougin-Degraef, J. Barbet, N. Michel, M. Cherel and A. Faivre-Chauvet, *Nucl. Med. Rev. Cent. East. Eur.*, 2011, **14**, 90–95.
- 16 K. A. Wood, W. L. Wong and M. I. Saunders, *Nucl. Med. Biol.*, 2008, **35**, 393–400.
- 17 J. A. Alawneh, R. R. Moustafa, S. T. Marrapu, U. Jensen-Kondering, R. S. Morris, P. S. Jones, F. I. Aigbirhio, T. D. Fryer, T. A. Carpenter, E. A. Warburton and J. C. Baron, *Eur. J. Nucl. Med. Mol. Imaging*, 2014, **41**, 736–744.
- 18 F. A. Rojas-Quijano, G. Tircso, E. T. Benyo, Z. Baranyai, H. T. Hoang, F. K. Kalman, P. K. Gulaka, V. D. Kodibagkar, S. Aime, Z. Kovacs and A. D. Sherry, *Chem. – Eur. J.*, 2012, **18**, 9669–9676.
- 19 K. Okuda, Y. Okabe, T. Kadonosono, T. Ueno, B. G. M. Youssif, S. Kizaka-Kondoh and H. Nagasawa, *Bioconjugate Chem.*, 2012, **23**, 324–329.
- 20 A. A. Bobko, T. D. Eubank, J. L. Voorhees, O. V. Efimova, I. A. Kirilyuk, S. Petryakov, D. G. Trofimov, C. B. Marsh, J. L. Zweier, I. A. Grigor'ev, A. Samouilov and V. V. Khramtsov, *Magn. Reson. Med.*, 2012, **67**, 1827–1836.
- 21 P. Kuppusamy, H. Q. Li, G. Ilangovan, A. J. Cardounel, J. L. Zweier, K. Yamada, M. C. Krishna and J. B. Mitchell, *Cancer Res.*, 2002, **62**, 307–312.
- 22 Q. N. Do, J. S. Ratnakar, Z. Kovacs and A. D. Sherry, *ChemMedChem*, 2014, **9**, 1116–1129.
- 23 E. L. Que and C. J. Chang, *Chem. Soc. Rev.*, 2010, **39**, 51–60.
- 24 P. B. Tsitovich, P. J. Burns, A. M. McKay and J. R. Morrow, *J. Inorg. Biochem.*, 2014, **133**, 143–154.
- 25 D. V. Hingorani, A. S. Bernstein and M. D. Pagel, *Contrast Media Mol. Imaging*, 2015, **10**, 245–265.
- 26 G. S. Loving, S. Mukherjee and P. Caravan, *J. Am. Chem. Soc.*, 2013, **135**, 4620–4623.
- 27 C. Tu, R. Nagao and A. Y. Louie, *Angew. Chem., Int. Ed.*, 2009, **48**, 6547–6551.
- 28 D. P. J. Pan, A. H. Schmieder, S. A. Wickline and G. M. Lanza, *Tetrahedron*, 2011, **67**, 8431–8444.
- 29 E. M. Gale, I. P. Atanasova, F. Blasi, I. Ay and P. Caravan, *J. Am. Chem. Soc.*, 2015, **137**, 15548–15557.
- 30 E. M. Gale, C. M. Jones, I. Ramsay, C. T. Farrar and P. Caravan, *J. Am. Chem. Soc.*, 2016, **138**, 15861–15864.
- 31 E. Boros, E. M. Gale and P. Caravan, *Dalton Trans.*, 2015, **44**, 4804–4818.
- 32 I. Bertini, C. Luchinat, G. Parigi and E. Ravera, *NMR of Paramagnetic Molecules – Applications to Metallobiomolecules and Models*, Elsevier, Amsterdam, 2017.
- 33 M. J. F. Calvete, S. M. A. Pinto, M. M. Pereira and C. F. G. C. Geraldes, *Coord. Chem. Rev.*, 2017, **333**, 82–107.
- 34 S. H. Koenig, R. D. Brown and M. Spiller, *Magn. Reson. Med.*, 1987, **4**, 252–260.
- 35 N. Schaeffle and R. Sharp, *J. Phys. Chem. A*, 2005, **109**, 3267–3275.
- 36 R. Sharp, L. Lohr and J. Miller, *Prog. Nucl. Magn. Reson. Spectrosc.*, 2001, **38**, 115–158.
- 37 D. Mansuy, *Cron. Chim.*, 2007, **10**, 392–413.
- 38 M. J. F. Calvete, M. Silva, M. M. Pereira and H. D. Burrows, *RSC Adv.*, 2013, **3**, 22774–22789.
- 39 C. A. Henriques, A. Fernandes, L. M. Rossi, M. F. Ribeiro, M. J. F. Calvete and M. M. Pereira, *Adv. Funct. Mater.*, 2016, **26**, 3359–3368.
- 40 L. Cuesta-Aluja, J. Castilla, A. M. Masdeu-Bulto, C. A. Henriques, M. J. F. Calvete and M. M. Pereira, *J. Mol. Catal. A: Chem.*, 2016, **423**, 489–494.
- 41 D. Dini, M. J. F. Calvete and M. Hanack, *Chem. Rev.*, 2016, **116**, 13043–13233.
- 42 C. A. Henriques, S. M. A. Pinto, J. Pina, C. Serpa, A. Fernandes, L. M. Rossi, M. F. Ribeiro, M. M. Pereira and M. J. F. Calvete, *Dalton Trans.*, 2016, **45**, 16211–16220.
- 43 A. T. Marques, S. M. A. Pinto, C. J. P. Monteiro, J. S. S. de Melo, H. D. Burrows, U. Scherf, M. J. F. Calvete and M. M. Pereira, *J. Polym. Sci., Part A: Polym. Chem.*, 2012, **50**, 1408–1417.
- 44 J. Roales, J. M. Pedrosa, M. G. Guillen, T. Lopes-Costa, S. M. A. Pinto, M. J. F. Calvete and M. M. Pereira, *Sens. Actuators, B*, 2015, **210**, 28–35.
- 45 D. Dini, M. Calvete, S. Vagin, M. Hanack, A. Eriksson and C. Lopes, *J. Porphyrins Phthalocyanines*, 2006, **10**, 1165–1171.
- 46 D. Dini, M. J. F. Calvete, M. Hanack, V. Amendola and M. Meneghetti, *Chem. Commun.*, 2006, 2394–2396.
- 47 S. M. A. Pinto, A. C. B. Neves, M. J. F. Calvete, A. R. Abreu, M. T. S. Rosado, T. Costa, H. D. Burrows and M. M. Pereira, *J. Photochem. Photobiol., A*, 2012, **242**, 59–66.
- 48 A. V. C. Simoes, S. M. A. Pinto, M. J. F. Calvete, C. M. F. Gomes, N. C. Ferreira, M. Castelo-Branco, J. Llop, M. M. Pereira and A. J. Abrunhosa, *RSC Adv.*, 2015, **5**, 99540–99546.
- 49 M. J. F. Calvete, A. V. C. Simoes, C. A. Henriques, S. M. A. Pinto and M. M. Pereira, *Curr. Org. Synth.*, 2014, **11**, 127–140.
- 50 S. M. A. Pinto, V. A. Tomé, M. J. F. Calvete, M. M. Pereira, H. D. Burrows, A. M. S. Cardoso, A. Pallier, M. M. C. A. Castro, E. Toth and C. F. G. C. Geraldes, *J. Inorg. Biochem.*, 2016, **154**, 50–59.
- 51 A. V. C. Simoes, A. Adamowicz, J. M. Dabrowski, M. J. F. Calvete, A. R. Abreu, G. Stochel, L. G. Arnaut and M. M. Pereira, *Tetrahedron*, 2012, **68**, 8767–8772.
- 52 D. J. Todd and J. Kay, *Annu. Rev. Med.*, 2016, **67**, 273–291.
- 53 M. Aschner, T. R. Guilarte, J. S. Schneider and W. Zheng, *Toxicol. Appl. Pharm.*, 2007, **221**, 131–147.
- 54 L. J. Jing, X. L. Liang, X. D. Li, Y. B. Yang and Z. F. Dai, *Acta Biomater.*, 2013, **9**, 9434–9441.
- 55 T. J. Zou, M. M. Zhen, D. Q. Chen, R. M. Li, M. R. Guan, C. Y. Shu, H. B. Han and C. R. Wang, *Dalton Trans.*, 2015, **44**, 9114–9119.
- 56 W. R. Cheng, I. E. Haedicke, J. Nofiele, F. Martinez, K. Beera, T. J. Scholl, H. L. M. Cheng and X. A. Zhang, *J. Med. Chem.*, 2014, **57**, 516–520.

- 57 T. D. MacDonald, T. W. Liu and G. Zheng, *Angew. Chem., Int. Ed.*, 2014, **53**, 6956–6959.
- 58 G. G. Westmeyer, Y. Emer, J. Lintelmann and A. Jasanoff, *Chem. Biol.*, 2014, **21**, 422–429.
- 59 I. E. Haedicke, T. Li, Y. L. K. Zhu, F. Martinez, A. M. Hamilton, D. H. Murrell, J. T. Nofiele, H. L. M. Cheng, T. J. Scholl, P. J. Foster and X. A. Zhang, *Chem. Sci.*, 2016, **7**, 4308–4317.
- 60 X. A. Zhang, K. S. Lovejoy, A. Jasanoff and S. J. Lippard, *Proc. Natl. Acad. Sci. U. S. A.*, 2007, **104**, 10780–10785.
- 61 T. Lee, X. A. Zhang, S. Dhar, H. Faas, S. J. Lippard and A. Jasanoff, *Chem. Biol.*, 2010, **17**, 665–673.
- 62 S. Aime, M. Botta, E. Gianolio and E. Terreno, *Angew. Chem., Int. Ed.*, 2000, **39**, 747–750.
- 63 M. Silva, A. Fernandes, S. S. Bebiano, M. J. F. Calvete, M. F. Ribeiro, H. D. Burrows and M. M. Pereira, *Chem. Commun.*, 2014, **50**, 6571–6573.
- 64 G. R. Friedermann, M. Halma, K. A. D. F. Castro, F. L. Benedito, F. G. Doro, S. M. Drechsel, A. S. Mangrich, M. D. Assis and S. Nakagaki, *Appl. Catal., A*, 2006, **308**, 172–181.
- 65 Q. Yu, Y. H. Liu, D. S. Liu and J. F. Li, *Dalton Trans.*, 2015, **44**, 9382–9390.
- 66 P. Turner and M. J. Gunter, *Inorg. Chem.*, 1994, **33**, 1406–1415.
- 67 W. Harhour, S. Dhifaoui, Z. Denden, T. Roisnel, F. Blanchard and H. Nasri, *Polyhedron*, 2017, **130**, 127–135.
- 68 R. Guillard, K. Perie, J. M. Barbe, D. J. Nurco, K. M. Smith, E. Van Caemelbecke and K. M. Kadish, *Inorg. Chem.*, 1998, **37**, 973–981.
- 69 M. A. C. deMedeiros, S. Cosnier, A. Deronzier and J. C. Moutet, *Inorg. Chem.*, 1996, **35**, 2659–2664.
- 70 E. J. Sun, Y. H. Shi, P. Zhang, M. Zhou, Y. H. Zhang, X. X. Tang and T. S. Shi, *J. Mol. Struct.*, 2008, **889**, 28–34.
- 71 L. Ruhlmann, A. Nakamura, J. G. Vos and J. H. Fuhrhop, *Inorg. Chem.*, 1998, **37**, 6052–6059.
- 72 F. C. Chen, S. H. Cheng, C. H. Yu, M. H. Liu and Y. O. Su, *J. Electroanal. Chem.*, 1999, **474**, 52–59.
- 73 M. A. Luna, F. Moyano, L. Sereno and F. D'Eramo, *Electrochim. Acta*, 2014, **135**, 301–310.
- 74 S. Romain, C. Duboc, F. Neese, E. Riviere, L. R. Hanton, A. G. Blackman, C. Philouze, J. C. Lepretre, A. Deronzier and M. N. Collomb, *Chem. – Eur. J.*, 2009, **15**, 980–988.
- 75 X. Q. Jiang, C. P. Gros, Y. Chang, N. Desbois, L. H. Zeng, Y. Cui and K. M. Kadish, *Inorg. Chem.*, 2017, **56**, 8045–8057.
- 76 A. Harriman, *J. Chem. Soc., Dalton Trans.*, 1984, 141–146.
- 77 A. J. Bard, in *Electrochemical Methods. Fundamentals and Applications*, Wiley, New York, 2nd edn, 2001.
- 78 S. E. Creager and R. W. Murray, *Inorg. Chem.*, 1987, **26**, 2612–2618.
- 79 J. A. Hodge, M. G. Hill and H. B. Gray, *Inorg. Chem.*, 1995, **34**, 809–812.
- 80 L. J. Boucher, *Coord. Chem. Rev.*, 1972, **7**, 289–329.
- 81 S. L. H. Rebelo, M. M. Pereira, M. M. Q. Simões, M. G. P. M. S. Neves and J. A. S. Cavaleiro, *J. Catal.*, 2005, **234**, 76–87.
- 82 E. Vancaemelbecke, W. Kutner and K. M. Kadish, *Inorg. Chem.*, 1993, **32**, 438–444.
- 83 L. Robitaille and L. J. Hoffer, *Nutr. J.*, 2016, **15**, 51.
- 84 M. Levine, C. ConryCantilena, Y. H. Wang, R. W. Welch, P. W. Washko, K. R. Dhariwal, J. B. Park, A. Lazarev, J. F. Graumlich, J. King and L. R. Cantilena, *Proc. Natl. Acad. Sci. U. S. A.*, 1996, **93**, 3704–3709.
- 85 Y. I. Turyan and R. Kohen, *J. Electroanal. Chem.*, 1995, **380**, 273–277.
- 86 C. E. Aitken, R. A. Marshall and J. D. Puglisi, *Biophys. J.*, 2008, **94**, 1826–1835.
- 87 L. H. Bryant, M. W. Hodges and R. G. Bryant, *Inorg. Chem.*, 1999, **38**, 1002–1005.
- 88 M. M. Williamson and C. L. Hill, *Inorg. Chem.*, 1987, **26**, 4155–4160.
- 89 D. Lieb, A. Zahl, T. E. Shubina and I. Ivanovic-Burmazovic, *J. Am. Chem. Soc.*, 2010, **132**, 7282–7284.
- 90 A. Budimir, K. Jozsef, F. Istvan, G. Lente, B. Istvan, I. Batinic-Haberle and M. Birus, *Dalton Trans.*, 2010, **39**, 4405–4410.
- 91 J. K. Moscicki, Y. K. Shin and J. H. Freed, *J. Chem. Phys.*, 1993, **99**, 634–649.
- 92 B. Drahos, J. Kotek, P. Hermann, I. Lukes and E. Toth, *Inorg. Chem.*, 2010, **49**, 3224–3238.
- 93 Y. Ducommun, K. E. Newman and A. E. Merbach, *Inorg. Chem.*, 1980, **19**, 3696–3703.
- 94 I. Bertini, F. Briganti, Z. C. Xia and C. Luchinat, *J. Magn. Reson., Ser. A*, 1993, **101**, 198–201.
- 95 A. Sour, S. Jenni, A. Orti-Suarez, J. Schmitt, V. Heitz, F. Bolze, P. L. de Sousa, C. Po, C. S. Bonnet, A. Pallier, E. Toth and B. Ventura, *Inorg. Chem.*, 2016, **55**, 4545–4554.
- 96 K. H. Chalmers, E. De Luca, N. H. M. Hogg, A. M. Kenwright, I. Kuprov, D. Parker, M. Botta, J. I. Wilson and A. M. Blamire, *Chem. – Eur. J.*, 2010, **16**, 134–148.
- 97 S. R. Davis, E. P. Quinlivan, P. W. Stacpoole and J. F. Gregory, *J. Nutr.*, 2006, **136**, 373–378.
- 98 K. P. Malikidogo, I. Da Silva, J. F. Morfin, S. Lacerda, L. Barantin, T. Sauvage, J. Sobilo, S. Lerondel, E. Toth and C. S. Bonnet, *Chem. Commun.*, 2018, **54**, 7597–7600.
- 99 S. A. Graves, R. Hernandez, J. Fonslet, C. G. England, H. F. Valdovinos, P. A. Ellison, T. E. Barnhart, D. R. Elema, C. P. Theuer, W. B. Cai, R. J. Nickles and G. W. Severin, *Bioconjugate Chem.*, 2015, **26**, 2118–2124.
- 100 A. M. D. R. Gonsalves, R. A. W. Johnstone, M. M. Pereira, A. M. P. de Santana, A. C. Serra, A. J. F. N. Sobral and P. A. Stocks, *Heterocycles*, 1996, **43**, 829–838.
- 101 D. Garreau and J. M. Saveant, *J. Electroanal. Chem.*, 1972, **35**, 309–331.
- 102 A. M. S. Cardoso, H. Faneca, J. A. S. Almeida, A. A. C. C. Pais, E. F. Marques, M. C. P. de Lima and A. S. Jurado, *Biochim. Biophys. Acta, Biomembr.*, 2011, **1808**, 341–351.